Annual Report

Electrooptical Devices

30 September 1985

Lincoln Laboratory

MASSACHUSETTS INSTITUTE OF TECHNOLOGY

LEXINGTON, MASSACHUSETTS

ADA193445

The views and conclusions contained in this document are those of the contractor and should not be interpreted as necessarily representing the official policies, either expressed or implied, of the United States Government.

The ESD Public Affairs Office has reviewed this report, and it is releasable to the National Technical Information Service, where it will be available to the general public, including foreign nationals.

This technical report has been reviewed and is approved for publication.

FOR THE COMMANDER

Hugh L. Southall

Hugh L. Southall, Lt. Col., USAF
Chief, ESD Lincoln Laboratory Project Office

MASSACHUSETTS INSTITUTE OF TECHNOLOGY
LINCOLN LABORATORY

ELECTROOPTICAL DEVICES

ANNUAL REPORT
TO THE
ROME AIR DEVELOPMENT CENTER

1 OCTOBER 1984 — 30 SEPTEMBER 1985

ISSUED 23 FEBRUARY 1988

LEXINGTON   MASSACHUSETTS

ABSTRACT

This report covers work carried out with the support of the Rome Air Development Center during the period 1 October 1984 through 30 September 1985.

The frequency response of an optical guided-wave GaAs interferometer has been measured. The bandwidth of the interferometer biased at a null point was 2.2 GHz, limited by parasitics. A small-signal bandwidth of ≈ 3 GHz can be inferred from this measurement for the case where the interferometer is biased to a linear operating point. This is the highest bandwidth yet reported for a guided-wave GaAs modulator.

A surface-emitting GaInAsP/InP laser has been developed in which a monolithically integrated parabolic mirror is used to up-deflect the output of a buried-heterostructure laser. A threshold current as low as 12 mA and a differential quantum efficiency as high as 46 percent have been obtained.

GaInAsP/InP distributed feedback lasers have been fabricated with a simple new design in which the grating is etched into the top of a mass-transported buried heterostructure. Single-frequency operation with side modes lower than -32 dB and threshold currents as low as 16 mA has been achieved.

Single-mode InP p^+-n^--n^+ slab-coupled rib waveguides capable of phase modulating, TE-polarized, 1.3-μm radiation have been fabricated. These guides should prove useful in the fabrication of two-guide coupler switches and interferometric modulators.

TABLE OF CONTENTS

LIST OF ILLUSTRATIONS

ELECTROOPTICAL DEVICES

I. FREQUENCY RESPONSE OF A GaAs GUIDE-WAVE ELECTROOPTIC INTERFEROMETER MODULATOR

We have recently reported a GaAs guided-wave electrooptic interferometric modulator.[1] These devices have the potential of being integrated with lasers for both high-speed analog and digital modulation. In this section, the frequency response of these interferometers is reported.

As shown in Figure I-1, the interferometer structure consists of a three-guide coupler[2-4] input section, the two active arms of the interferometer, and a three-guide coupler output section. The three-guide couplers consist of three closely spaced single-mode n^-–n^+ slab-coupled waveguides,[5] while the two active arms are single-mode p^+–n^-n^+ slab-coupled waveguides.[6] The input three-guide coupler acts as a power divider. Power input into the center guide is divided equally between the two outside guides in a coupling length, L_C. The output three-guide coupler acts as a power combiner. For power input into the two outside guides, the in-phase components of the two inputs are combined in the center guide in a length, L_C, while the out-of-phase components
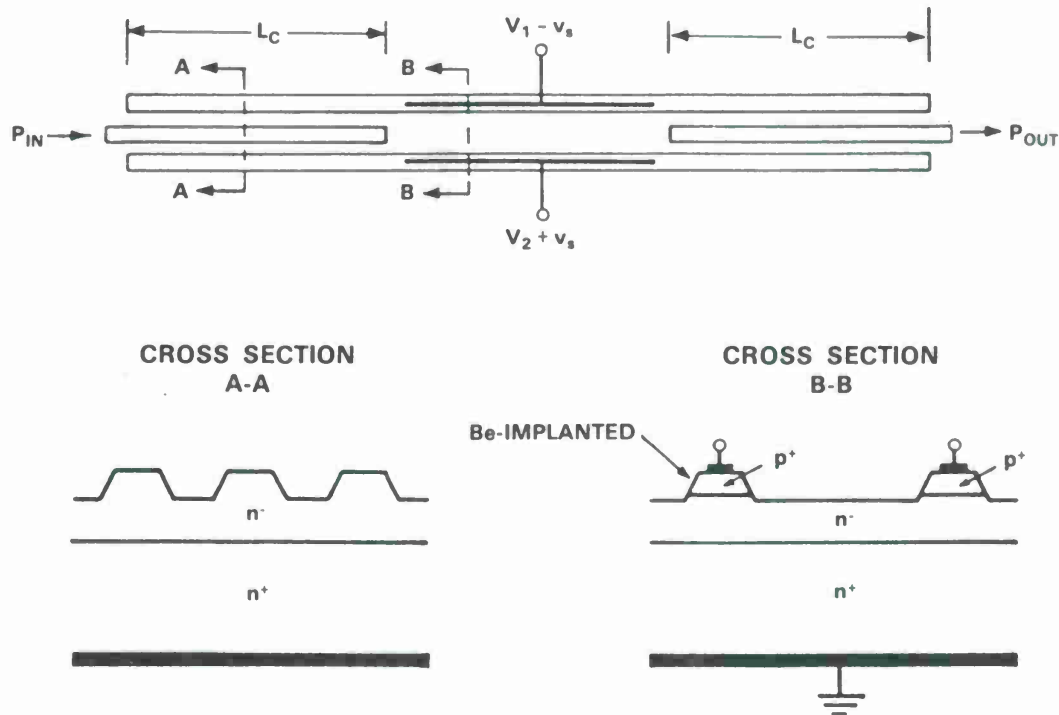

Figure I-1. Schematic illustration of GaAs electrooptic interferometric modulator.

1

remain in the outside guide. The effective index in the active arms may be changed via the electrooptic effect by changing the bias on the p-n junctions. The phase of the output of either or both arms of the interferometer may therefore be changed, resulting in modulation of the signal out of the center guide of the output three-guide coupler.

The actual interferometers were fabricated on a GaAs wafer consisting of an unintentionally doped n^--epilayer ($n \leqslant 5 \times 10^{15}$ cm^{-3}) grown on an n^+-substrate ($n \approx 2 \times 10^{18}$ cm^{-3}) oriented 5° off the $\{100\}$. A multi-energy Be implant[7] was used to form the p^+-region. Following implantation annealing, the rib-waveguide interferometer structure was etched using a Ti-etch mask. An SiO_2 layer was then deposited and ohmic contacts applied to the p^+-ribs and the back of the n^+-substrate. In these experiments, the length of the output three-guide coupler was determined by cleaving instead of photolithographically so that the output of all three guides could be observed. Additional information on the fabrication procedure can be found in Reference 1.

To test the interferometer, radiation from a single-mode GaInAsP/InP double-heterojunction laser operating at 1.3 μm was end-fired coupled into the center guide of the input three-guide coupler. The electric field of the input light was polarized parallel to the plane of the slab.

The output of a recently fabricated interferometer with 2-mm-long active arms biased for maximum and minimum output in the center guide is shown in Figures I-2(a) and (b), respectively. The output is more symmetric and the extinction ratio is higher than obtained on initial devices.[1] Maximum output in the center guide is not obtained with the same bias (typically zero) on both arms because of a built-in optical phase difference (of about 25°) between the two arms. The output three-guide coupler is slightly shorter than a coupling length, resulting in a small
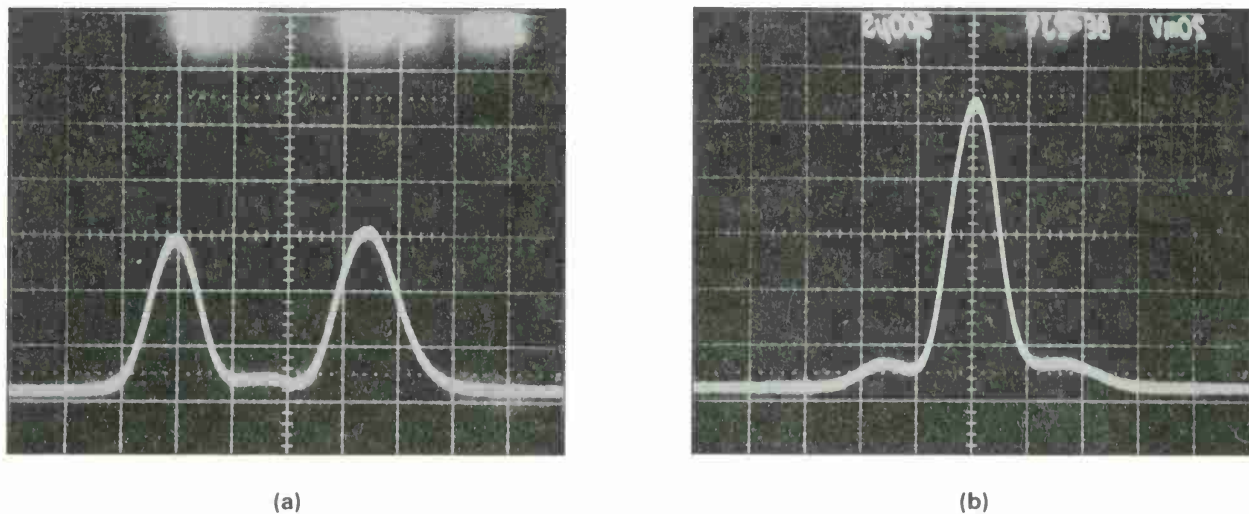

(a)　　　　　　　　　　　　　(b)

Figure I-2. Scanned output of interferometer: (a) biased for a maximum output in the center guide, and (b) biased for a minimum output in the center guide.

85891-2

amount of power remaining in the outside guides when the interferometer is biased for maximum output in the center guides. When biased for minimum output in the center guide, about 1.5 percent of the power remained in the center guide for an extinction ratio of ≈ 18 dB.

Swept-frequency measurements[8] were used to determine the frequency response of the above interferometer. For these measurements, the interferometer was biased by means of a bias "T" to a V_π point, i.e., a point at which there is a minimum in the output of the center guide, and a swept high-frequency signal modulated by a 2-kHz square wave was applied to one arm of the interferometer. The output of the center guide was detected by a photodiode and a lock-in amplifier reference to the 2-kHz square wave used to obtain a high signal-to-noise ratio output signal. The frequency response obtained from these measurements corresponds to the electrical response of the interferometer electrode structure. As shown in Figure I-3, the measured 3-dB electrical bandwidth of the interferometer (point A) is ≈ 2.2 GHz. Because the transfer function of the interferometer with applied bias is nonlinear, the electrical-to-optical small-signal response depends on the bias point. If the interferometer is biased to operate in the linear optical range,
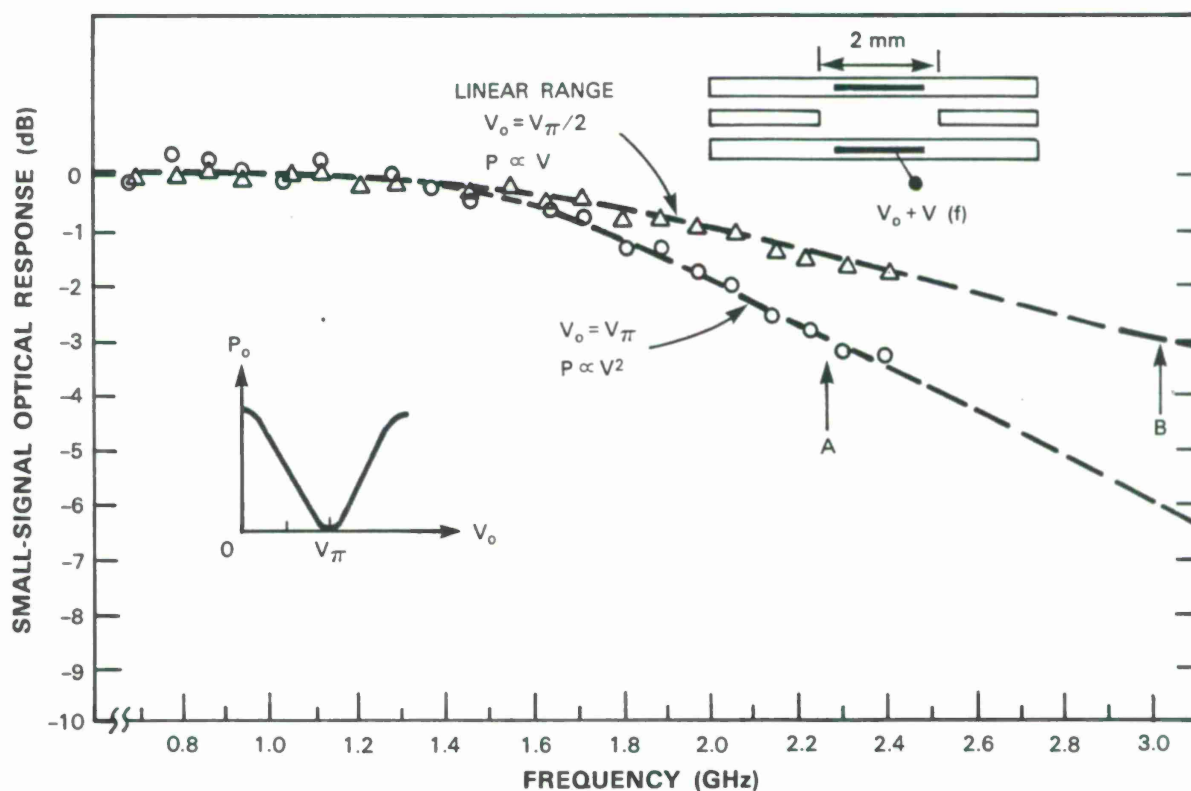
Figure I-3.   *Frequency response of interferometers obtained from swept-frequency measurements: (O) optical response obtained with interferometer biased at a V_p point; (Δ) square root of above when biased at a linear optical response point $V_\pi/2$. The electrical bandwidth of the interferometer electrode structure is ≈ 2.2 GHz (point A), which translates into a linear optical bandwidth of ≈ 3.0 GHz (point B).*

3

i.e., a $V_\pi/2$ point, the optical response is equal to the square root of that obtained from the swept-frequency measurements at a V_π point. The square root of the electrical response is therefore also plotted in Figure I-3 and indicates a linear optical bandwidth (point B) of 3.0 GHz.

The bandwidth of these interferometers is currently limited by parasitics. The major limiting parasitic is the resistance of the long narrow metal contacts on top of the p^+-ribs. The end-to-end resistance of the metallization on the device measured is $\approx 60\ \Omega$. This high resistance means that the active arm electrode must be treated as a lossy transmission line or distributed RC circuit. In addition, the bonding pads, which run out over the SiO_2 insulating layer, add a parasitic capacitance of ≈ 0.25 pF. It should be possible to significantly reduce both of these parameters by modifications in the fabrication procedures so that the linear optical bandwidth of an interferometer with 2-mm-long active arms should increase toward the calculated maximum in a 50-Ω system, namely ≈ 12 GHz; here transit time limitations also become important.

<div align="right">

J.P. Donnelly   G.A. Ferrante
N.L. DeMeo   K.B. Nichols

</div>

II. A SURFACE-EMITTING GaInAsP/InP LASER WITH LOW THRESHOLD CURRENT AND HIGH EFFICIENCY

Surface-emitting diode lasers are of considerable interest for a variety of new applications such as monolithic two-dimensional arrays and optical interconnects for integrated circuits. However, results reported to date[9,10] have had a variety of difficulties. In this work, a new approach is introduced that has resulted in a surface-emitting GaInAsP/InP laser with performance comparable to the best of the conventional edge-emitting ones.

As illustrated in Figure II-1, the surface emission is achieved by adding a 45° mirror to a previously developed buried-heterostructure laser with "transported" mirrors.[11] As shown in Figure II-2, the 45° mirror is fabricated at the same time as the transported mirror by partially removing the phosphosilicate glass (PSG) mask during the selective chemical etching procedure[11]
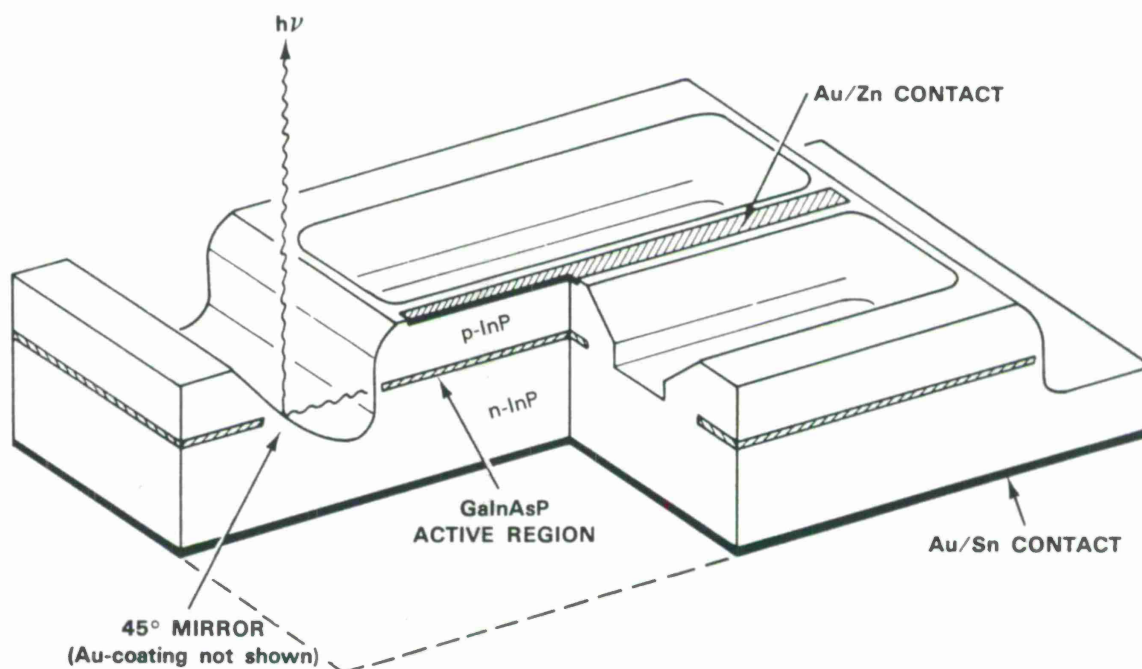
Figure II-1. *A schematic cutaway view of the surface-emitting GaInAsP/InP laser. The surface emission is achieved by adding a 45° mirror to a previously developed buried-heterostructure laser with transported mirrors.*

(a) ETCH A GROOVE

PSG MASK

InP:Zn CAP LAYER
p = 1.2 × 10¹⁸ cm⁻³

InP:Zn
CLADDING LAYER
p ≃ 2.5 × 10¹⁷

GaInAsP
ACTIVE LAYER
n ≤ 1 × 10¹⁷

InP:Sn BUFFER LAYER, n = 2 × 10¹⁸

InP:Sn SUBSTRATE, n ≤ 1 × 10¹⁸

GaInAsP
ETCH-STOP
LAYER (optional)
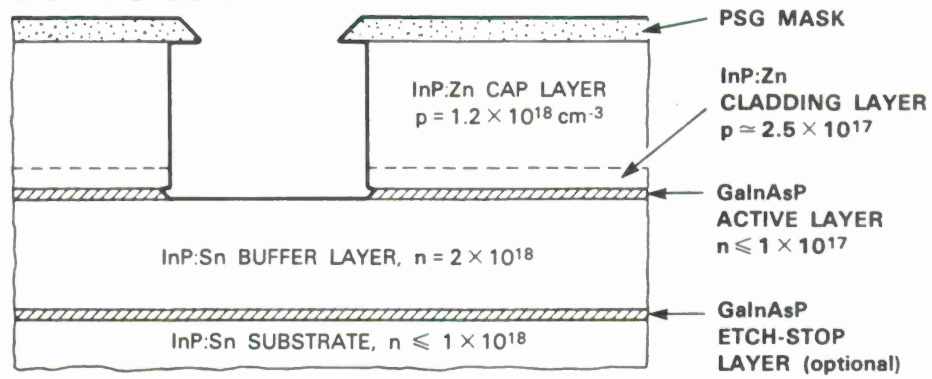
(b) PARTIALLY REMOVE MASK AND REPEAT ETCHING

s

t_1

t_2

(c) MASS TRANSPORT

690 TO 715°C
H_2 AND PH_3

a

I

II

III

IV

F

σ
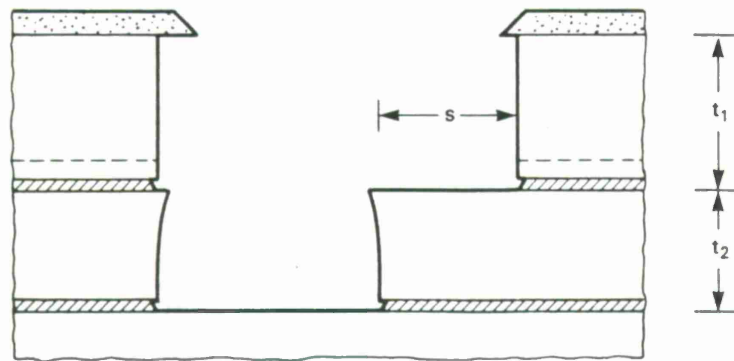
Figure II-2. Simultaneous fabrication of the 45° (parabolic) and the transported mirrors. The dotted curve is a parabola with its focus at point F.

6

85891-5

such that a stair-structure is formed and subsequently mass-transported. By designing the stair-structure such that regions I, II, III, and IV in Figure II-2(c) have equal areas, the resulting mirror profile can approximate a portion of a parabola and can therefore reduce the laser beam divergence. It can be verified directly by integration that the equal-area requirement is fulfilled to within a few percent by choosing

$$t_1 = (2 + \frac{8}{3}\,\epsilon - \frac{8}{9}\,\epsilon^2)\,\sigma$$

$$t_2 - (2 - \frac{4}{3}\,\epsilon - \frac{32}{9}\,\epsilon^2 - \frac{64}{9}\epsilon^3)\,\sigma$$

and

$$s = (2 + \frac{2}{3}\,\epsilon + \frac{4}{9}\,\epsilon^2)\,\sigma \qquad ,$$

where t_1, t_2, s, σ, and a are defined in Figure II-2 and $\epsilon \equiv \sigma/2a$. [The parabola shown as a dotted curve in Figure II-2(c) can be expressed as $y = x^3/2a$.] To fully collect the diverging laser output and to achieve a narrow diffraction-limited beam, larger parabolic mirrors are desired but necessitate higher m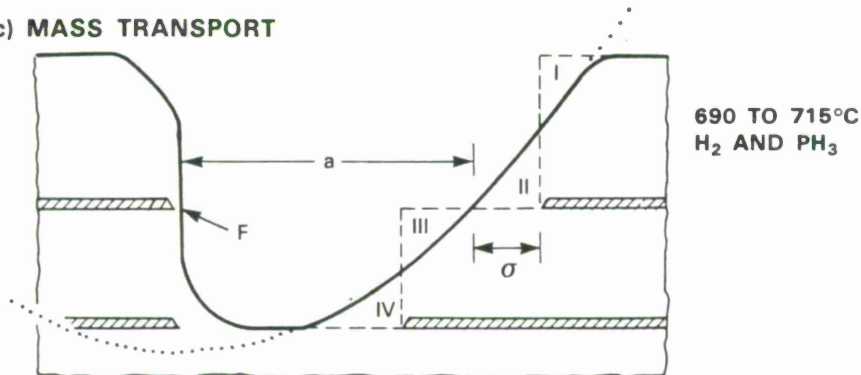ass-transport temperatures. For example, 715°C was needed to fully smooth the parabolic mirror in Wafer 685 with $t_1 \simeq 2.7\ \mu m$, $t_2 \simeq 2.2\ \mu m$, and $s \simeq 2.5\ \mu m$. Figure II-3 shows a scanning-electron micrograph of a cross-sectional view of an approximately parabolic mirror and a transported mirror (cf. Figure II-2(c)].
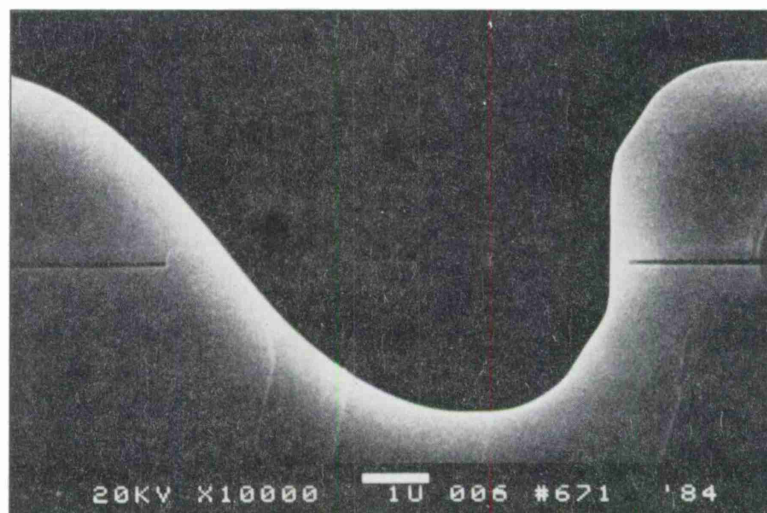
Figure II-3. SEM photograph of an approximately parabolic mirror (left) and a transported mirror (right).

7

The wafer is then metallized by using the previously described procedure,[11,12] except that, instead of sputtering, the Ti and Au layers are deposited by using angle evaporations in order to avoid coating the front laser mirror (the one facing the parabolic mirror). Note that the laser resonator as shown in Figure II-1 consists of two transported mirrors; no cleaved mirror is used. After metallization, the rear mirror is coated by PSG/Au layers, while the front one is only covered by the PSG of an estimated 0.17 μm thickness.

Surface-emitting lasers with low threshold current and high efficiency have been obtained with good yield. For example, 70 percent of the 26 devices tested (without preselection) from Wafer 685 showed pulsed threshold currents of 12 to 18 mA. Figure II-4 shows a CW light-current characteristic with a threshold current of 12 mA and an initial differential quantum efficiency of 46 percent. A typical far-field pattern is shown in Figure II-5, in which a narrow beam
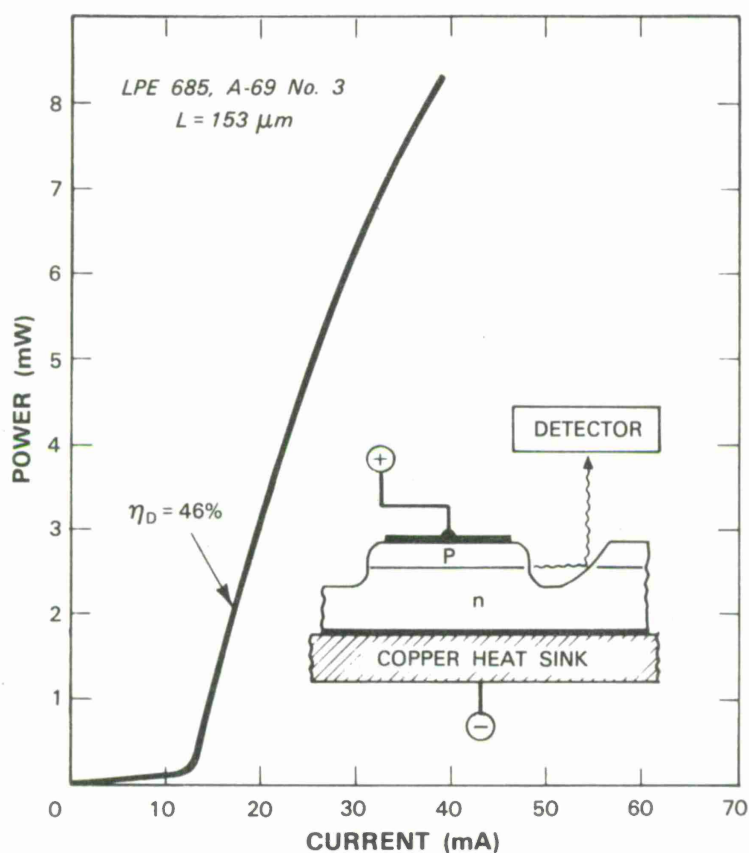
Figure II-4. Light output vs current characteristic of a surface-emitting GaInAsP/InP laser. The laser is mounted p-side up on a copper heat sink as shown in the insert.
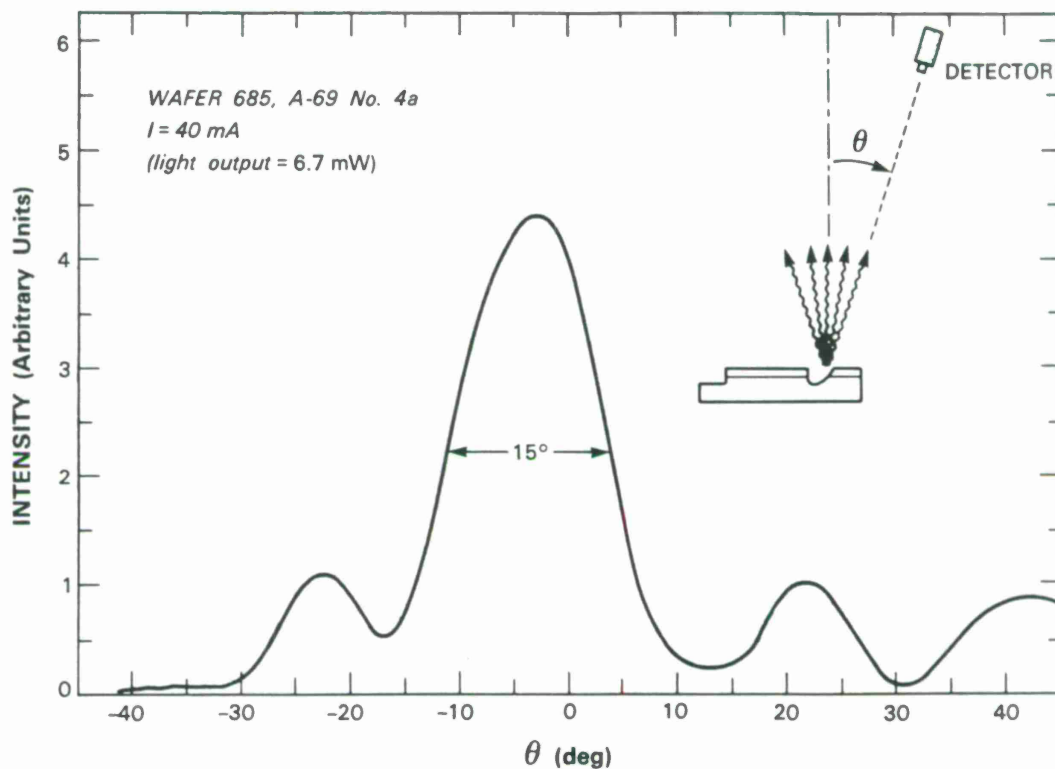
Figure II-5. Far-field pattern of a surface-emitting GaInAsP/InP laser.

(15° angular width for the main lobe) nearly perpendicular to the substrate surface is demonstrated. Other tested devices show angular widths as small as 12°, which is considerably narrower than the corresponding far-field patterns (typically ≥30°) of the conventional edge-emitting lasers[13-17] and is close to the diffraction-limited angular width estimated from the present parabolic mirror size.

In conclusion, a high-performance surface-emitting GaInAsP/InP diode laser has been developed which is very promising for a variety of new applications in integrated optoelectronics.

Z.L. Liau
J.N. Walpole

9

III. A NOVEL GaInAsP/InP DISTRIBUTED FEEDBACK LASER

In recent years considerable effort has been devoted to the development of GaInAsP/InP distributed feedback (DFB) lasers for use as stable single-frequency sources in fiber optic communications.[18-23] In this work we describe a novel device design which offers high performance and considerable fabrication simplicity.

As illustrated in Figure III-1, the device consists of a mass-transported buried heterostructure[12,24] with a thin p-InP cap layer and a wide mesa on which a grating corrugation is etched in the middle, with Au/Zn alloyed contacts formed on each side. Sufficient coupling between the guided mode and the grating corrugation occurs if the InP cap layer is approximately 1-μm thick. The first-order grating corrugation with a periodicity of 2028 Å and tooth height of approximately 2500 Å is formed by using contact x-ray lithography[25] (with a holographically generated mask pattern) and ion-beam-assisted etching using chlorine gas.[26] The wafer is then coated with a phosphosilicate glass (PSG) layer 0.4-μm thick (not shown in Figure III-1, and a pair of stripe openings are defined in the PSG on top of the laser mesa for Au/Zn alloyed contacts. The rest of the metallization and dicing procedures are similar to those described previously.[12] Each finished device has a cleaved front facet where the output power is measured; the rear is either cleaved or saw-cut.
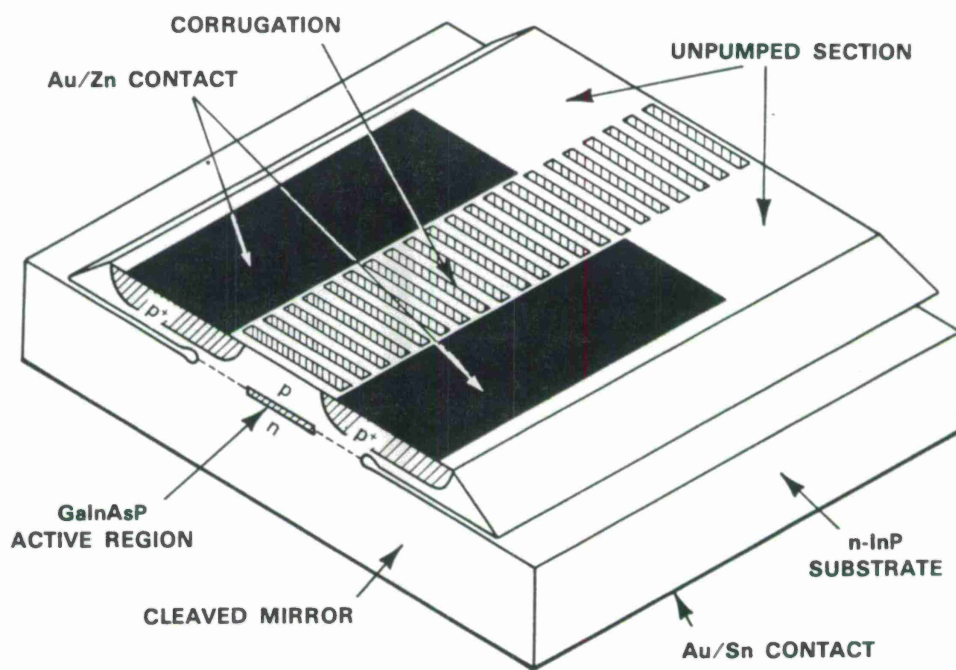
Figure III-1. A schematic drawing of the GaInAsP/InP distributed feedback laser.

11

Devices fabricated with a relatively long cavity (546 and 241 μm for pumped and unpumped sections, respectively) and saw-cut end show room-temperature pulsed threshold currents as low as 16 mA. Figure III-2(a) and (b) shows CW emission spectra of a device just above its lasing threshold. As evident in Figure III-2(a), the dominant lasing mode with a wavelength of 1.3098 μm is located on the shorter-wavelength side of the apparent spontaneous emission spectrum. This is a strong indication that the device is lasing in a DFB mode, since the Fabry-Perot
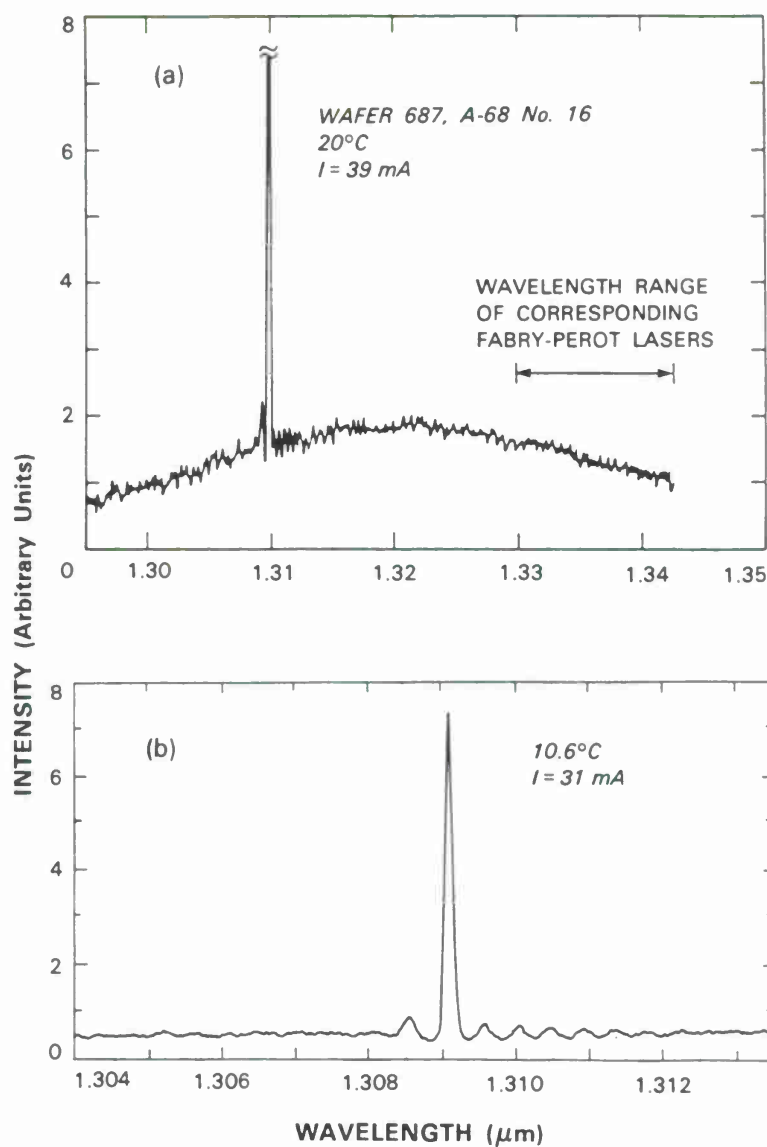
Figure III-2.   *Emission spectra of one device just above lasing threshold at (a) 20°C and (b) 10.6°C. In (a) lasing modes are shown located on shorter-wavelength side of apparent spontaneous emission spectrum. Expanded wavelength scale in (b) shows more details of lasing spectrum.*

modes should be located on the other side of the spontaneous spectrum where the gain maximum occurs. Indeed, Fabry-Perot mode operation at wavelengths of 1.33 to 1.34 μm was observed in shorter devices cleaved from the same wafer but without the unpumped section and saw-cut end. (Since the present DFB resonance wavelength is approximately 260 Å away from the gain maximum, the Fabry-Perot mode can have a lower threshold current in devices without the unpumped section and saw-cut end.) Figure III-2(b) shows a similar spectrum at 10.6°C and on different scales. Note that the threshold current drops to 31 mA. The series of peaks are likely the DFB modes, with the dominant one just outside the stop band.[18,19]

At higher currents the dominant mode continues to grow, and the other DFB modes are at −37 dB when the current is 60 mA (which is approximately 1.54 times the threshold current I_{th}), as shown in Figure III-3. However, a pair of modes of unknown origin with a −32-dB intensity are observed at ±50 Å of the dominant DFB mode, as evident in Figure III-3.

Shorter devices with smaller unpumped sections and both ends cleaved show room-temperature CW threshold currents as low as 13.5 mA but with more complicated mode behaviors. A device with pumped and unpumped sections of 318 and 152 μm, respectively, showed a CW threshold current of 16 mA at room temperature and single-frequency operation (with side modes estimated at −30 dB) up to at least 2.5 I_{th} (with an output power of 2.8 mW), but with a mode hop from λ = 1.3054 to 1.3092 μm at 1.6 I_{th}. Other devices with little or no unpumped sections lase in Fabry-Perot modes in the spectral region of 1.33 to 1.34 μm, but still show considerably better mode purity than similar devices fabricated without the grating. (The latter also lase at wavelengths of 1.33 to 1.34 μm.)

It is worth noting that the present device is considerably simpler than more conventional DFB lasers[18-23] in terms of the waveguide and current-confinement structures and fabrication procedures. In particular, the grating is fabricated after the wafer growth is completed. This not only avoids the problems associated with growth over the grating,[28,29] but also allows the wafer to be more thoroughly characterized before the grating is fabricated.

One potential problem of the present device is a possible leakage current I_H flowing through the InP pn homojunctions in the transported regions.[24] (The homojunctions are illustrated as dashed-line segments in Figure III-1.) This current leakage has been analyzed previously for other mass-transported buried-heterostructure lasers and has been shown to be capable of causing a saturation of light output at high current.[24] A similar analysis has been carried out for the present structure,* in which the current I_Q flowing from the Au/Zn contacts to the quaternary active region and the corresponding voltage distribution are modeled by using a conformal mapping technique, as illustrated in Figure III-4. This analysis yields the forward-bias voltage along the homojunctions, which can in turn be used to estimate I_H. For small values of I_Q the calculated I_H is negligible, but its importance grows with increasing I_Q. The value of I_Q when I_H = 0.1

---

* The present calculation is somewhat different from that in Reference 24 because of the device geometry and the relative importance of the electron drift current.
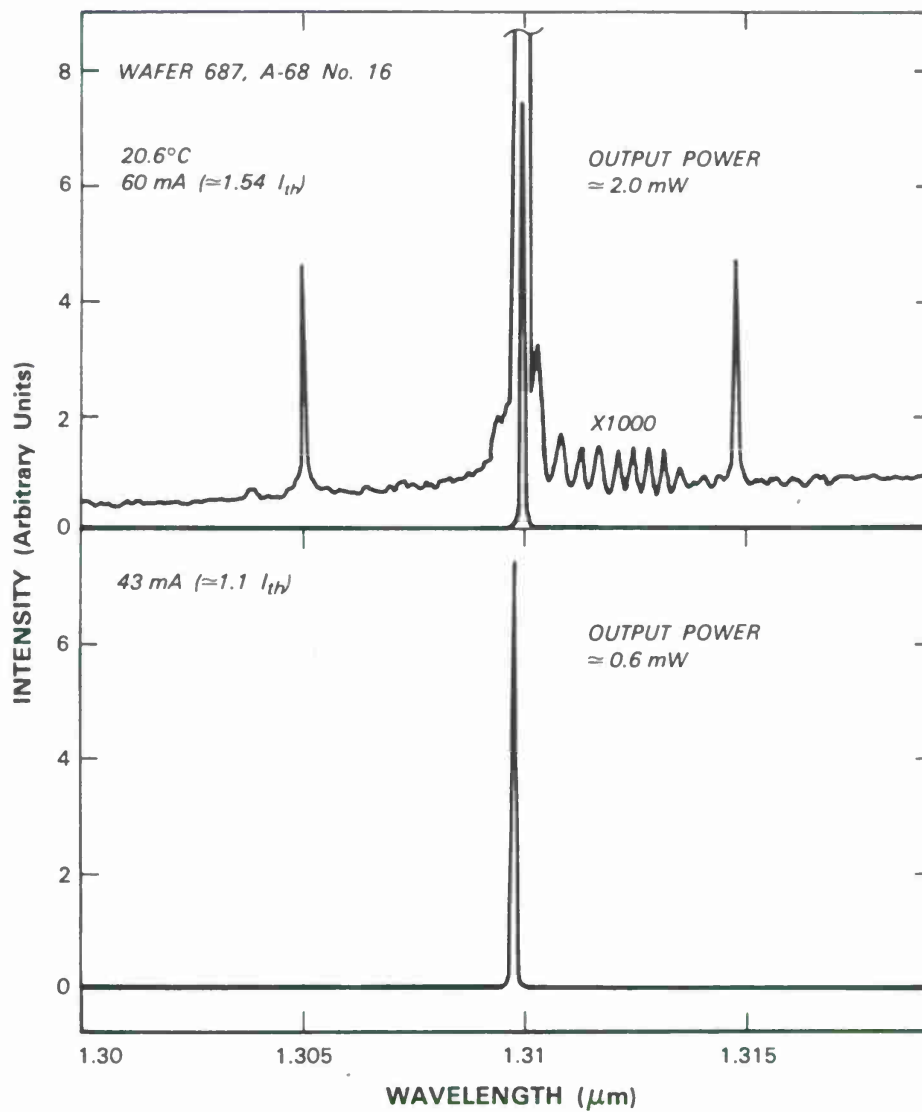
Figure III-3. Emission spectra of device at 20.6°C and two different currents above threshold. Note that, at I = 1.54 I$_{th}$, sidemodes are lower than –32 dB.

p = 1 × 10^18 cm^-3
PUMPED SECTION = 300 μm
CURRENT = 50 mA

1 μm

Zn-DIFFUSED REGION

Au/Zn CONTACT

1.06   1.10

1.02

p⁺   p⁺

ACTIVE REGION

V ≡ 0.0 V IN n-InP BUFFER LAYER
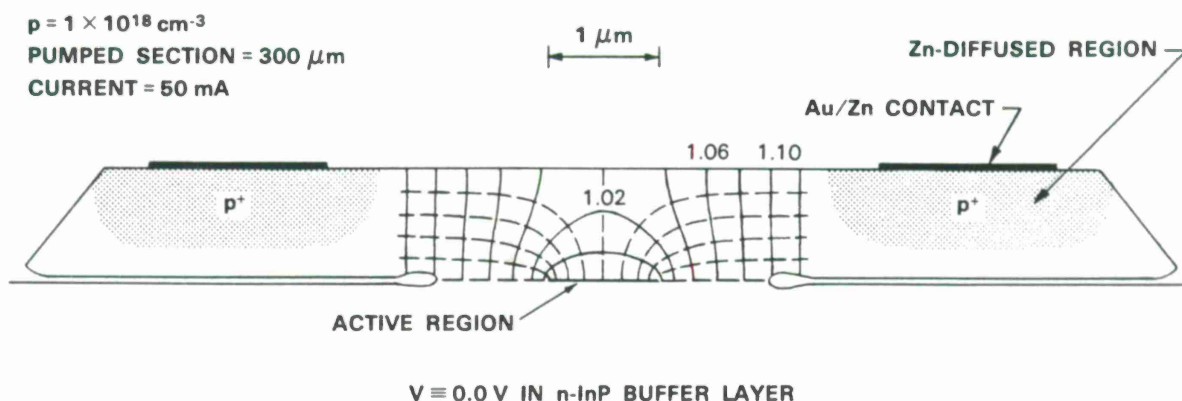
Figure III-4.   Calculated current and voltage distributions near active region in present structure. Dashed curves are streamlines of current flowing into active region. Solid curves are equipotentials, with numbers labeling voltage values in volts.

I_Q is designated as I_1 and has been calculated for various device parameters; e.g., I_1 = 74 mA is obtained for the device of Figure III-4. I_1 can be increased considerably by using a higher p-doping, narrower transported regions, a closer alignment of the Zn-diffused p⁺ regions to the quaternary, or a larger pumped-section length. It is worth noting that, if the device were fabricated with an n-type mesa on a p-type substrate, there would be negligible voltage buildup due to high conductivity of n-type InP. However, the p-doping on the substrate side would need optimization in order to enable very high current operation.

In conclusion, a GaInAsP/InP DFB laser has been realized in a simple new design in which the grating is fabricated on top of a mass-transported buried heterostructure. Threshold currents as low as 16 mA have been obtained, and still lower threshold current can possibly be achieved when the DFB resonance wavelength and the gain maximum are better matched. Further optimization of the doping scheme, the transported region width, and ohmic contact alignment is needed for high-power capability.

Z.L. Liau   N.L. DeMeo
D.C. Flanders   D.K. Astolfi
J.N. Walpole

15

IV. SINGLE-MODE InP OPTICAL WAVEGUIDE
CAPABLE OF PHASE MODULATION

Single-mode optical waveguides in which the effective index can be modulated via the electrooptic effect are necessary components of integrated-optic switches and modulators. In this section an InP single-mode p^+-n^--n^+ slab-coupled rib waveguide capable of phase modulating TE-polarized 1.3-μm radiation is described. It should be possible to fabricate two-guide coupler switches[30,31] and interferometric modulators[32,33] in InP using guides of this type.

A schematic cross section of a single-mode p^+-n^--n^+ InP slab-coupled rib waveguide is shown in Figure IV-1. The InP wafer used to fabricate these waveguides consisted of a (100)-oriented n^+-substrate and a 5.5-μm-thick n-type layer with a carrier concentration of $\approx 2 \times 10^{16}$ cm^{-3} grown by liquid phase epitaxy. To form the p^+ ribs, the wafer was implanted with a multi-energy Be-implanted schedule and annealed at 750°C, which produced a 1.5-μm-deep p^+ layer with a uniform carrier concentration of $\approx 2 \times 10^{18}$ cm^{-3} (Reference 34). Rib waveguides approximately 5 μm wide were then formed by etching through the p^+ implanted layer into the epitaxial layer to a total depth of about 2 μm. The waveguides were oriented for propagation along a (011) direction. An SiO$_2$ layer was deposited on top of the wafer and Au/Mg and Au/Sn ohmic contacts were applied to the p^+ ribs and the back of the n^+ substrate, respectively. The input and output
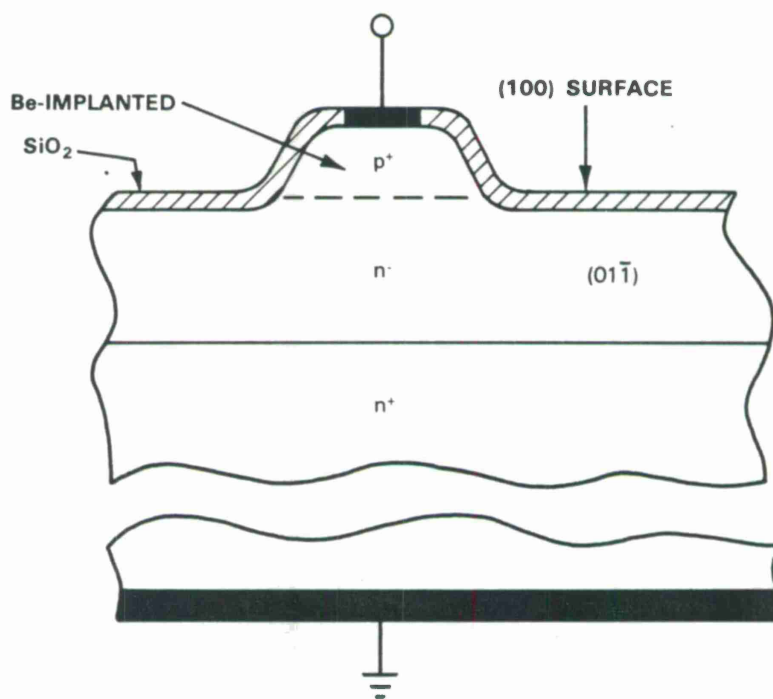

Figure IV-1.   Schematic of single-mode p^+–n–n^+ InP slab-coupled rib waveguide.

faces of the waveguide were then cleaved. These p^+-n^-n^+ InP waveguides are similar to the GaAs waveguides recently used in a high-frequency interferometer.[32,33] While the propagation loss of these guides was not measured in detail, a comparison of their transmitted power with that of guides of similar dimensions with known loss coefficients indicates that the loss per unit length is of the order of 1.5 to 2.0 cm^{-1} at 1.3 μm.

To determine the modulation characteristics of these waveguides, radiation from a single-mode GaInAsP/InP double-heterojunction laser operating at 1.3 μm was passed through a polarizer and end-fired coupled into the cleaved end face of one of the waveguides. The input radiation was polarized (nominally at 45° to the perpendicular) so that approximately an equal amount of TE- and TM-like radiation was excited in the guide. The output of the waveguide was passed through an analyzer and focused on a Ge photodiode.

Figure IV-2 shows the relative outputs of a 5-mm-long waveguide vs reverse bias on the p^+-n junction with the analyzer either parallel or perpendicular to the input polarization. Both curves approximate an offset cosine function of applied voltage. The maximum output with the analyzer parallel to the input polarization (minimum output with the analyzer perpendicular to the input polarization) does not occur at zero bias, because at low fields the velocity of the TE-like mode is slightly slower than that of the TM-like mode. Reverse biasing the p^+-n junction decreases the
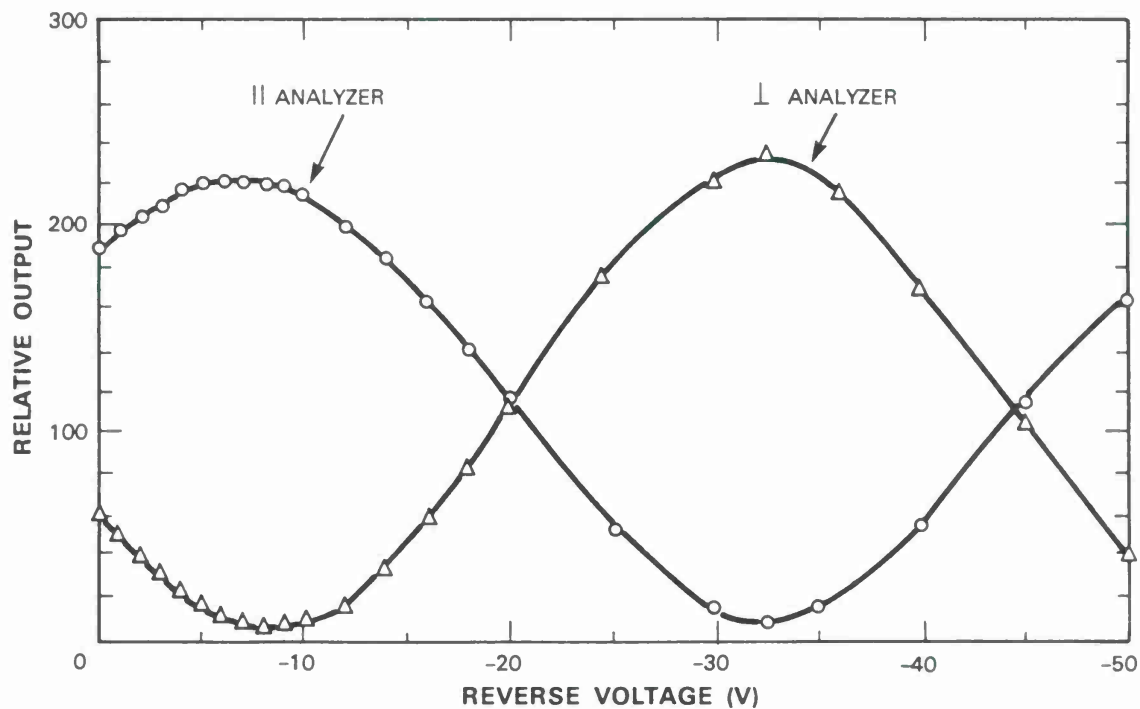

Figure IV-2.   Relative output vs reverse bias of 5-mm-long p^+-n-n^+ InP slab-coupled rib waveguide with approximately equal amounts of TE- and TM-like radiation excited at input and an output analyzer parallel and perpendicular to input polarization.

18

refractive index in the plane of the junction [i.e., the (011) direction], but leaves the index perpendicular to the plane of the junction [i.e., the (100) direction] unaffected.[35,36] Therefore, the velocity of the TE-like mode increases with reverse bias, while that of the TM-like mode is, at least to first order, not affected. This results in a change in phase of the TE-like mode relative to that of the TM-like mode at the output face, and produces the observed variation in relative output. The extinction ratio is about 16.5 dB. This relatively low value was obtained primarily because the amounts of TE- and TM-like radiation in the guide were not exactly equal. Extinction ratios in couplers and interferometers where only the TE-like radiation is excited should be considerably higher.

A voltage difference of about 25 V is required to produce a π phase shift in the TE-like mode, i.e., to go from a maximum to a minimum in the relative output of either curve shown in Figure IV-2. Using simple approximations for both the electric field shape in the p-n junction and the field shape of the TE-like optical mode, a rough estimate of $\approx 1.5 \times 10^{-10}$ cm/V for the electrooptic coefficient η_{41} was obtained from the measured voltage difference. This value is in reasonable agreement with the η_{41} value of 1.3×10^{-10} cm/V reported for InP at 1.35 μm by Tada and Suzuki.[37]

J.P. Donnelly   F.J. O'Donnell
N.L. DeMeo   S.H. Groves

REFERENCES

1. J.P. Donnelly, N.L. DeMeo, G.A. Ferrante, K.B. Nichols, and F.J. O'Donnell, Appl. Phys. Lett. **45** 360 (1984).

2. K. Iwasaki, S. Kurazano and K. Itakuma, Electron. Commun. Jpn. **58-C**, 100 (1975).

3. H.A. Haus and C.G. Fonstad, Jr., IEEE J. Quantum Electron., **QE-17**, 2321 (1981).

4. J.P. Donnelly, N.L. DeMeo, and G.A. Ferrante, J. Lightwave Technol. **LT-1**, 417 (1984).

5. E.A. Marcatili, Bell Syst. Tech. J. **53** 645 (1974).

6. F.J. Leonberger, J.P. Donnelly, and C.O. Bozler, Appl. Phys. Lett. **28**, 616 (1976), DDC AD-A027103.

7. J.P. Donnelly, F.J. Leonberger, and C.O. Bozler, Appl. Phys. Lett. **28**, 706 (1976), DDC AD-A028457.

8. S. Uehara, Appl. Opt. **17**, 68 (1978).

9. K. Iga, H. Soda, T. Terakado, and S. Shimizu, Electron. Lett. **19**, 457 (1983).

10. Y. Itaya, T. Matsuoka, Y. Nakano, Y. Suzuki, K. Kuroiwa and T. Ikegami, Electron. Lett. **18**, 1006 (1982).

11. Z.L. Liau, J.N. Walpole, and D.Z. Tsang, Appl. Phys. Lett. **44**, 945 (1984).

12. Z.L. Liau and J.N. Walpole, Appl. Phys. Lett. **40**, 568 (1982), DTIC AD-A121779.

13. Y. Itaya, Y. Suematsu, S. Katayama, K. Kishino, and S. Arai, Jpn. J. Appl. Phys. **18**, 1795 (1979).

14. M. Hirao, A. Doi, S. Tsuji, M. Nakamura, and K. Aiki, J. Appl. Phys. **51**, 4539 (1980).

15. R.J. Nelson, P.D. Wright, P.A. Barnes, R.L. Brown, T. Cella, and R.G. Sobers, Appl. Phys. Lett. **36**, 358 (1980).

16. H. Ishikawa, H. Imai, T. Tanahashi, K. Hori, and K. Takahei, IEEE J. Quantum Electron. **QE-18**, 1704 (1982).

17. I. Mito, M. Kitamura, K. Kobayashi, S. Murata, M. Seki, Y. Odagiri, H. Nishimoto, M. Yamaguchi, and K. Kobayashi, IEEE J. Lightwave Technol. **LT-1**, 195 (1983).

18. K. Utaka, S. Akiba, K. Sakai, and Y. Matsushima, IEEE J. Quantum Electron. **LT-1**, 195 (1983).

19. Y. Itaya, T. Matsuoka, K. Kuroiwa, and T. Ikegami, IEEE J. Quantum Electron. **QE-20**, 230 (1984), and references therein.

20. H. Okuda, Y. Hirayama, J. Kinoshita, H. Furuyama, and Y. Uematsu, Electron. Lett. **19**, 941 (1983).

21. L.D. Westbrook, A.W. Nelson, P.J. Fiddyment, and J.S. Evans, Electron. Lett. **20**, 225 (1984).

22. M. Kitamura, M. Yamaguchi, S. Murata, I. Mito, and K. Kobayashi, Electron. Lett. **20**, 595 (1984), and references therein.

23. B. Broberg, F. Koyama, Y. Tohmori, and Y. Suematsu, Electron. Lett. **20**, 692 (1984).

24. Z.L. Liau, J.N. Walpole, and D.Z. Tsang, IEEE J. Quantum Electron. **QE-20**, No. 8, 855 (1984), DTIC AD-A149328.

25. D.C. Flanders, J. Vac. Sci. Technol. **16** 1615 (1979), DTIC AD-A090070.

26. N.L. DeMeo, J.P. Donnelly, F.J. O'Donnell, M.W. Geis, and K.J. O'Connor, presented at the Conference on Ion-Beam Modification of Materials '84, Ithaca, New York, 1984; published in Nuclear Instr. & Methods in Physics Research **B7**, 814 (1985).

27. Z.L. Liau and J.N. Walpole, Appl. Phys. Lett. **40**, 568 (1982); Semiannual Technical Summary "Electrooptical Devices", Lincoln Laboratory, MIT (31 March 1985.

28. A.W. Nelson, L.D. Westbrook, and J.S. Evans, Electron. Lett. **19**, 34 (1983).

29. J. Kinoshita, H. Okuda, and Y. Uematsu, Electron. Lett. **19**, 215 (1983).

30. A. Carenco, L. Menegaux, and N.T. Lenh, Appl. Phys. Lett. **40**, 653 (1982).

31. F.J. Leonberger, J.P. Donnelly, and C.O. Bozler, Appl. Phys. Lett. **29**, 65 (1976), DDC AD-A037627.

32. J.P. Donnelly, N.L. DeMeo, G.A. Ferrante, K.B. Nichols, and F.J. O'Donnell, Appl. Phys. Lett. **45**, 360 (1984).

33. J.P. Donnelly, N.L. Demeo, G.A. Ferrante, and K.B. Nichols, IEEE J. Quantum Electron. **QE-21**, 18 (1985).

34. J.P. Donnelly and C.A. Armiento, Appl. Phys. Lett. **34**, 96 (1979).

35. S. Namba, J. Opt. Soc. AM **51**, 76 (1961).

36. A. Yariv, *Quantum Electronics* (Wiley, New York, 1967) pp. 300-306.

37. K. Tada and N. Suzuki, Jpn. J. Appl. Phys. **19**, 2295 (1980).

APPENDIX A

A High-Frequency GaAs Optical Guided-Wave Electrooptic Interferometric Modulator

J. P. DONNELLY, N. L. DEMEO, G. A. FERRANTE, AND K. B. NICHOLS

Abstract—The characteristics and frequency response of a GaAs monolithic guided-wave interferometric modulator operating at 1.3 μm are presented. The interferometer consists of three-guide coupler input and output sections and single-mode p^+-n^--n^+ slab-coupled rib-waveguide active arms. The measured electrical bandwidth of an interferometer with 2 mm long active arms was 2.2 GHz and limited by parasitics. This corresponds to a small signal optical bandwidth of ≈ 3.0 GHz when the interferometer is biased in a linear portion of the optical output versus voltage characteristics. Reduction of parasitics should result in a substantial increase in the bandwidth of these devices.

W E have recently reported a monolithic guided-wave GaAs inteferometer [1] capable of modulation via the electrooptic effect. Interferometers of this type have the potential of being integrated with lasers for both high-speed analog and digital modulation. In this paper, additional results on these interferometers including frequency-response measurements are reported. The measured bandwidth of these devices, as far as we have been able to determine, is the highest so far achieved on any semiconductor guided-wave modulator.

As shown in Fig. 1, the interferometer structure consists of a three-guide coupler [2]-[8] input section, the two active arms of the interferometer and a three-guide coupler output section. The three-guide couplers consist of three closely spaced single-mode n^--n^+ slab-coupled waveguides [5], while the two active arms are single-mode p^+-n^--n^+ slab-coupled waveguides [6]. The input three-guide coupler acts as a power divider. Power input into the center guide is divided equally between the two outside guides in a coupling length L_c. The output three-guide coupler acts as a power combiner. For power input into the two outside guides, the in-phase components of the two inputs are combined in the center guide in a length L_c, while the out-of-phase components remain in the outside guide. The effective index in the active arms may be changed via the electrooptic effect by changing the bias on the p-n junctions. The phase of the output of either or both arms of the interferometer may therefore be changed, resulting in modulation of the signal out of the center guide of the output three-guide coupler.

The actual interferometers were fabricated on a GaAs wafer consisting of a 4.2 μm thick unintentionally doped n^--epilayer ($n \leqslant 5 \times 10^{15}$ cm^{-3}) grown on an n^+-substrate ($n \approx 2 \times 10^{18}$ cm^{-3}) oriented 5° off the {100}. Following a selective multi-energy Be ion implantation and postimplantation anneal to form 2 mm long p^+-regions [7], the rib-waveguide interferom-
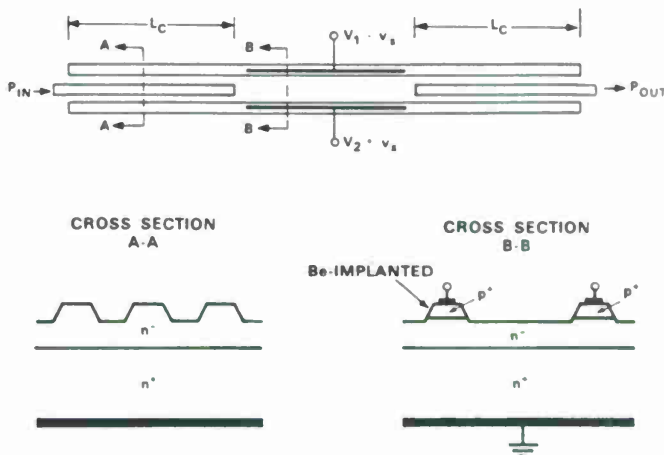
Fig. 1. Schematic illustration of the GaAs electrooptic interferometric modulator.

eter structure was etched with the waveguides in a (011) direction. An SiO$_2$ layer was then deposited, ohmic contacts applied, and the input and output faces of the interferometer cleaved. For these experiments, the length of the output three-guide coupler was determined by cleaving, instead of photolithographically, so that the output of all three guides could be observed. Additional information on the fabrication can be found in [1].

The cleaved end face of a three-guide coupler is shown in Fig. 2. The guide width and spacings are about 5 and 4 μm, respectively. The etch depth is ≈ 1.5 μm. The end face was stained so that the n^--n^+ interface could be seen. For these dimensions, the coupling length L_c is ≈ 3.2 mm [4]. Length of couplers not exactly equal to a coupling length will result in incomplete coupling and, therefore, power loss. It should be possible using photolithographic techniques to control coupling lengths to 10–15 percent, resulting in power losses due to coupling length variations of less than 6 percent.

Two top views of the active arms of the interferometer are shown in Fig. 3. The top photomicrograph shows the two waveguide arms where the contact metalization on the p^+-regions begins. The spacing between the two arms of the interferometer is sufficiently large so that coupling between them can be neglected. The bottom photomicrograph shows a contact bonding pad which runs out over the SiO$_2$ insulating layer. For practical considerations, the bonding pads for the top and bottom electrodes are offset and, therefore, are not in the center of the active arms. The arms of another interferometer can be seen below the contact pad. The reverse
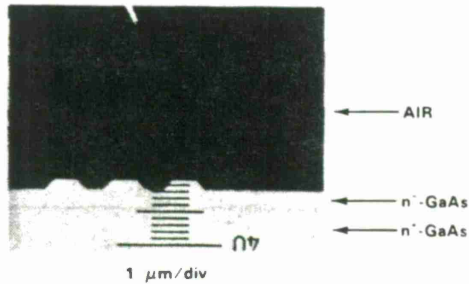
Fig. 2. Cleaved end face of three-guide coupler section. The face has been stained so the n⁻-n⁺ interface could be observed.
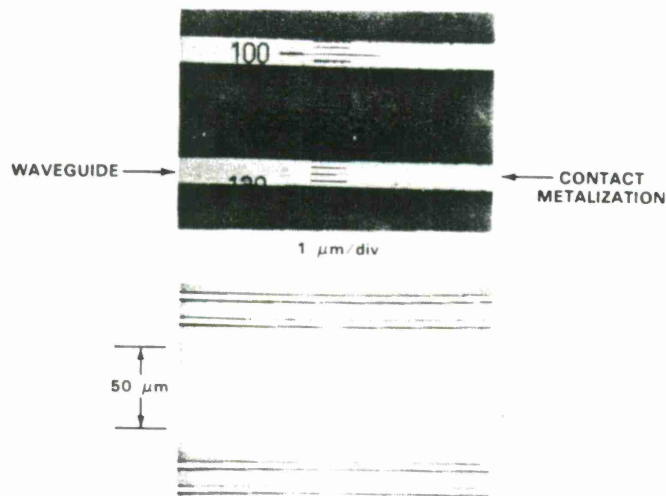

Fig. 3. Top view of p⁺-n⁻-n⁺ active arms of interferometer. Top: photomicrograph showing portion where metalization on p⁺-ribs begins. Bottom: photomicrograph showing bonding pad which runs out over SiO_2 insulating layer.
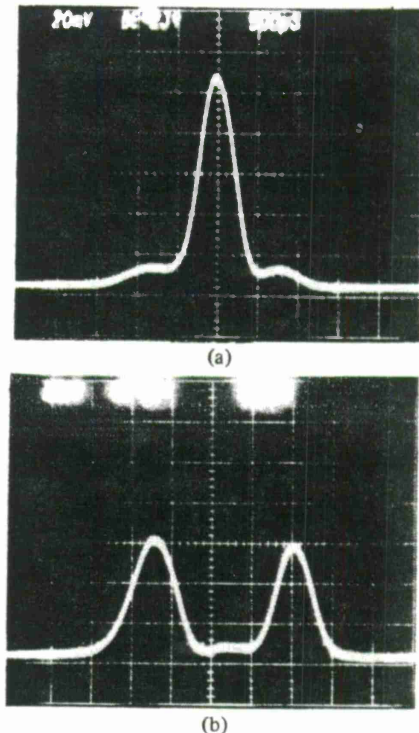

Fig. 4. Scanned output of interferometer (a) biased for a maximum output in the center guide and (b) biased for a minimum output in the center guide.

Fig. 5. Output of center guide of interferometer with 2 mm long active arms versus bias on each arm. The dc offset between the two arms is due to a built-in optical length difference between the arms.

current-voltage characteristics of the active arms' $p^+-n^--n^+$ junctions typically show leakage currents in the nanoampere range close to the ≈ 70 V breakdown.

To test an interferometer, radiation from a single-mode GaInAsP/InP double-heterojunction laser operating at 1.3 μm was endfired coupled into the center guide of the input three-guide coupler. The electric field of the input light was polarized parallel to the plane of the slab. The output of the interferometer was magnified and focused on a pin-hole aperture placed in front of a Ge photodiode. The output image could be scanned across the pin-hole using a scanning mirror, or any part of it could be precisely positioned on the pin-hole.

The scanned output of a recently fabricated interferometer, with 2 mm long active arms biased near the points for maximum and minimum output in the center guide, is shown in Fig. 4(a) and (b), respectively. The output is more symmetric and the extinction ratio is higher than obtained on initial devices [1]. Maximum output in the center guide is not obtained with the same bias (typically zero) on both arms because of a built-in optical length difference between the two arms as discussed below. The output three-guide coupler was cleaved slightly shorter than a coupling length, resulting in a small amount of power remaining in the outside guides when the interferometer is biased for maximum output in the center

guides [Fig. 4(a)]. When biased near the point for minimum output in the center guide, almost all the power is divided between the two outside guides. As can be seen in Fig. 5, which plots the output of the center guide versus bias on each arm, about 1.5 percent of the maximum output power remains in the center guide at a minimum for an extinction ratio of ≈ 18 dB. Fig. 5 is discussed more fully below. Losses in this interferometer are less than 2 dB greater than in a single straight n^--n^+ rib guide [4]. The additional losses are due to absorption in the active arms' p^+-ribs and incomplete coupling in the three-guide couplers. Total losses (neglecting input and output losses at the cleaved end face) are, therefore, about 5 dB.

As indicated in Fig. 1, these interferometers can be operated in a push–pull configuration. For this mode of operation in an ideal interferometer, one arm would be biased to $V_\pi/4$ and the other to $3V_\pi/4$, where V_π is the voltage difference required on one arm of the interferometer to go from a maximum to minimum output in the center guide. An ac signal v_s with a peak amplitude of $V_\pi/4$ applied in a push–pull fashion as shown in Fig. 1 would then result in 100 percent modulation. On an actual interferometer, the actual dc biases V_1 and V_2 have to be adjusted from these values to compensate for any built-in optical length differences between the two arms. For the interferometer discussed above there is as shown in Fig. 5, approximately a 10 V difference in bias between the two arms for the same output, indicating a built-in phase difference of $\approx 25°$. Voltage offsets between the two arms, from only a few volts to about 20 V, have been observed. These small optical path differences between the two arms of the interferometers are caused by slight differences in waveguide dimensions (including epitaxial layer thickness) and/or carrier concentration variations. It should be noted that built-in phase differences of this type are also generally observed in LiNbO$_3$ interferometers. In addition to the phase difference, it appears from the data shown in Fig. 5 that the differential change in phase with voltage of the two arms of the interferometer can also be slightly different.

Swept-frequency measurements [8] were used to determine the frequency response of these interferometers. For these measurements, the interferometer was biased by means of a bias "T" to a V_π point, i.e., a point at which there is a minimum in the output of the center guide, and a swept high-frequency signal modulated by a 2 kHz square wave applied to one arm of the interferometer. The output of the center guide was detected by the photodiode and a lock-in amplifier referenced to the 2 kHz square wave used to obtain a high signal-to-noise ratio output signal. When biased to a V_π point, the small signal optical response is proportional to the square of that portion of the signal voltage, which actually appears across the active arm of the interferometer $V^2(f)$. The frequency response obtained from these measurements therefore corresponds to the electrical response of the interferometer electrode structure. As shown in Fig. 6, the measured electrical bandwidth of the interferometer (point A) ≈ 2.2 GHz. Because the transfer function of the interferometer with applied bias is nonlinear, the electrical-to-optical small-signal response depends on the bias point. If the interferometer is biased to operate in the linear-optical range, i.e., a $V_\pi/2$ point, where the small-signal optical output is proportional to $V(f)$, the optical response is equal to the square root of that obtained from the swept-frequency measurements at a V_π point. The square root of the electrical response is therefore also plotted in Fig. 5. From this plot, the linear-optical bandwidth (point B) is ≈ 3.0 GHz. (Note that this is the - 6 dB point on the electrical response curve.)

The bandwidth of these interferometers is currently limited by parasitics. The major limiting parasitic is the resistance of the long narrow thin (≈ 3000 Å thick) metal contacts on top of the p$^+$-ribs. The end-to-end resistance of the metalization on the device measured is ≈ 60 Ω. Because of this high resis-
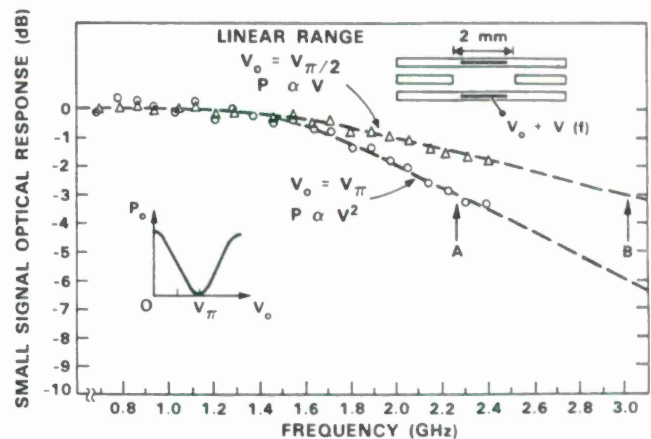

Fig. 6. Frequency response of interferometers obtained from swept-frequency measurements: (O) actual data obtained with interferometer biased at a V_π point. (Δ) square root of data to show response when biased at a linear optical response $V_\pi/2$ point. The electrical bandwidth of the interferometer electrode structure is ≈ 2.2 GHz (point A), which corresponds to a linear optical bandwidth of ≈ 3.0 GHz (point B).

tance, the active arm electrode cannot be treated as a lumped element capacitor and must be treated as a lossy transmission line or distributed RC circuit. In addition, the bonding pads which run out over the SiO$_2$ insulating layer add a parasitic capacitance of ≈ 0.25 pF. It should be possible to significantly reduce both of these parasitics by modifications in the fabrication procedures. Planarization of the interferometer structure with polyimide or another insulator, prior to contact metalization, should significantly reduce the parasitic bonding pad capacitance and permit thicker and possibly wider contact metalization on top of the p$^+$-rib which would reduce series resistance. Multiple feeds could also be used to reduce series resistance. With reduction of these parasitics, the linear optical bandwidth of an interferometer with 2 mm long active arms should increase toward the calculated maximum in a 50 Ω system of ≈ 12 GHz, where transit time limitations also become important.

It should also be possible to reduce both the length of the input and output three-guide coupler and the drive voltage requirements by reducing the dimensions of the waveguide. The drive voltage requirements can also be reduced somewhat by reducing the carrier concentration of the n$^-$-epilayer, since the p$^+$-n$^-$-n$^+$ diode would then operate in the punch-through mode even at low reverse biases. For a three-guide coupler with a slab thickness of 1.7 μm, a rib height (etch depth) of 1.5 μm, and guide widths and spacings of 3.5 μm, coupling lengths should be in the range of 1.6–1.8 mm. With an n$^-$-epilayer concentration of $\approx 10^{14}$ cm^{-3}, V_π voltages as low as ≈ 15 V for 2 mm long active arms should then be possible.

In conclusion, it has been shown that monolithic electro-optic guided-wave interferometers in GaAs are capable of modulation in the multigigahertz range. The measured electrical bandwidth of 2.2 GHz (linear optical bandwidth of ≈ 3.0 GHz) of these devices is presently limited by device parasitics. It should be possible to significantly reduce these parasitics by modifications in the contact metalization procedures. Linear optical bandwidths should then increase

27

significantly and could approach the calculated maximum bandwidth in a 50 Ω system of ≈ 12 GHz for a device with 2 mm long active arms.

REFERENCES

[1] J. P. Donnelly, N. L. DeMeo, G. A. Ferrante, K. B. Nichols, and F. J. O'Donnell, "An optical guided-wave gallium arsenide monolithic interferometer," *Appl. Phys. Lett.*, vol. 45, pp. 360–362, Aug. 15, 1984.

[2] K. Iwasaki, S. Kurazano, and K. Itakuma, "The coupling of modes in three dielectric slab waveguides," *Electron. Commun. Japan.*, vol. 58-C, no. 8, pp. 100–108, 1975.

[3] H. A. Haus and C. G. Fonstad, Jr., "Three-waveguide coupler for improved sampling and filtering," *IEEE J. Quantum Electron.*, vol. QE-17, pp. 2321–2325, Dec. 1981.

[4] J. P. Donnelly, N. L. DeMeo, and G. A. Ferrante, "Three guide optical couplers in GaAs," *J. Lightwave Technol.*, vol. LT-1, pp. 417–424, June 1984.

[5] E. A. Marcatili, "Slab-coupled waveguides," *Bell Syst. Tech. J.*, vol. 53, no. 4, pp. 645–674, Apr. 1974.

[6] F. J. Leonberger, J. P. Donnelly, and C. O. Bozler, "Low-loss GaAs $p^+n^-n^+$ three dimensional optical waveguides," *Appl. Phys. Lett.*, vol. 18, pp. 616–619, May 15, 1976.

[7] J. P. Donnelly, F. J. Leonberger, and C. O. Bozler, "Uniform-carrier-concentration p-type layers in GaAs produced by beryllium ion implantation," *Appl. Phys. Lett.*, vol. 28, pp. 706–708, June 15, 1976.

[8] S. Uehara, "Calibration of optical modulator frequency response with application to signal level control," *Appl. Opt.*, vol. 17, pp. 68–71, Jan. 1, 1978.

APPENDIX B

29

Surface-emitting GaInAsP/InP laser with low threshold current and high efficiency

Z. L. Liau and J. N. Walpole

Lincoln Laboratory, Massachusetts Institute of Technology, Lexington, Massachusetts 02173-0073

A buried-heterostructure laser has been developed whose output is deflected to a direction perpendicular to the substrate surface by a monolithically integrated 45° (parabolic) mirror. The latter is fabricated by smoothing a chemically etched multistep structure using a mass-transport phenomenon. The present devices show threshold current as low as 12 mA, differential quantum efficiency as high as 47% and a surface-emitting far-field pattern with a main lobe as narrow as 12°.

Surface-emitting lasers (i.e., diode lasers with emission directed perpendicular to the substrate) are of considerable interest for a variety of applications such as monolithic two-dimensional arrays and optical interconnects for integrated circuits. Moreover, unlike the conventional (edge-emitting) lasers, the surface-emitting ones do not require cleaving or dicing and are therefore potentially advantageous for batch processing and on-wafer testing. However, previous attempts for realizing surface-emitting lasers, which include the use of a vertical cavity[1,2] and a second-order grating,[3,4] have experienced difficulties and devices with good performance have not yet been obtained. In this work, a new approach is introduced and a surface-emitting GaInAsP/InP laser has been developed with performance comparable to the best of the conventional edge-emitting ones.

As illustrated in Fig. 1, the surface emission is achieved by adding an approximately parabolic mirror to a buried-heterostructure laser with "transported mirrors."[5] The parabolic mirror is fabricated by using selective chemical etching and mass transport in a technique very similar to that used to fabricate the transported mirror.[5] In fact, both kinds of mirrors are needed in the present device and are fabricated at the same time as shown in Fig. 2. After a groove has been formed by using the previously described two-step selective chemical etching procedure[5] [Fig. 2(a)], the phosphosilicate glass (PSG) mask is partially removed on one side of the groove. The selective chemical etching procedure is then repeated which produces a stair structure on one side of the groove and a nearly vertical profile on the other side, as shown in Fig. 2(b). For easier control of the etched profile, a GaInAsP etch-stop layer[6] is often used as indicated in Fig. 2. After etching, the wafer is then stripped of the PSG and loaded into a furnace system for mass transport[5,7] at a temperature of 690–740 °C in an H_2 and PH_3 atmosphere, in order to form a nearly parabolic mirror out of the stair structure and a transported mirror out of the nearly vertical profile [Fig. 2(c)].

A mirror profile which exactly follows the parabola [the dotted curve in Fig. 2(c)] with its focus near the buried-heterostructure laser output is expected to reduce the laser beam divergence. In order to achieve this desired profile, we have designed the stair structure such that regions I, II, III, and IV between the parabola and the stair structure have approximately equal areas, as illustrated in Fig. 2(c). With the parabola expressed as $y = x^2/2a$, it can be verified direct-

ly by integration that the equal-area requirement is fulfilled to within 3% (for $\epsilon < 0.13$) by using

$$t_1 = (2 + \tfrac{8}{3}\epsilon - \tfrac{8}{3}\epsilon^2)\sigma,$$
$$t_2 = (2 - \tfrac{4}{3}\epsilon - \tfrac{32}{9}\epsilon^2 - \tfrac{64}{9}\epsilon^3)\sigma,$$

and

$$s = (2 + \tfrac{2}{3}\epsilon + \tfrac{4}{3}\epsilon^2)\sigma,$$

where t_1, t_2, s, σ, and a are defined in Fig. 2 and $\epsilon \equiv \sigma/2a$. Note that this simplified analysis has ignored the rounded edges generally observed on actual mirrors [see Fig. 3(b) below].

Figure 3 shows optical micrographs of the cross-sectional view of a wafer before and after the mass transport. It has been found that mass-transport temperatures higher than those previously used[5,7,8] are necessary to smooth out larger stair structures. Nevertheless, the wafer surface remains mirror-smooth without a sign of degradation after mass transport at temperatures up to 740 °C, the highest used in this work. Mirror profiles close to the desired parabolic shape have been obtained for the stair structures which follow the design rule described in the previous paragraph. In contrast, large deviations from the design result in mirror profiles of markedly different curvatures or angles. To maintain the mirror to within ± 5° of the desired 45° angle, for example, the deviation of s from the optimum value must be less than an estimated ± 0.5 μm. (This estimation has been made for the present mirror size by using the above-mentioned equal-area requirement.)

After the mirrors have been formed, the wafer is metal-
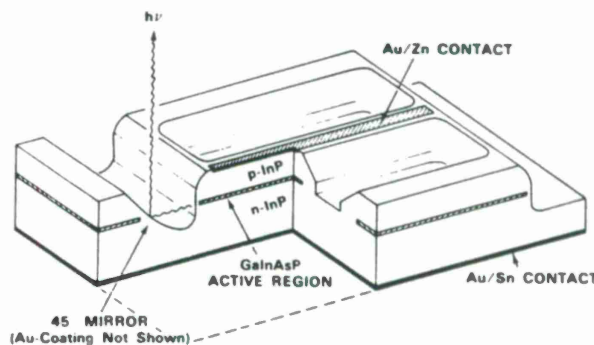

FIG. 1. Schematic cut-away view of the surface-emitting GaInAsP/InP laser. This device consists of a buried-heterostructure laser with a monolithically integrated 45° (parabolic) mirror.
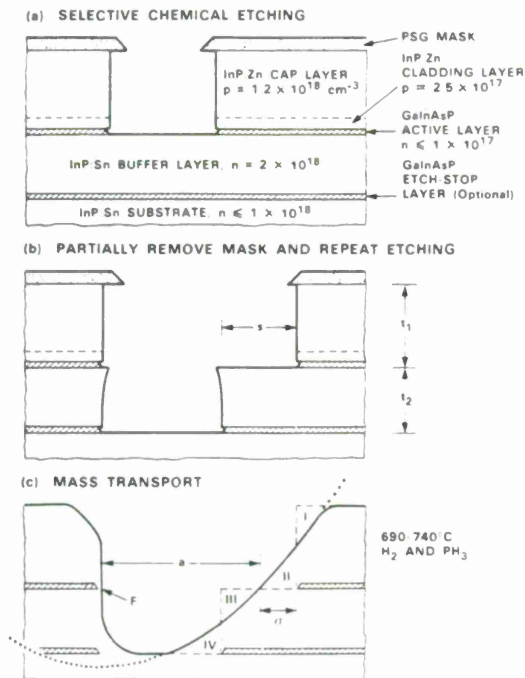
FIG. 2. Simultaneous fabrication of the parabolic and transported mirrors. The dotted curve in part (c) is a parabola with its focus at F.

lized by using the previously described procedure,[5,7] except that instead of sputtering, the Ti and Au layers are deposited by using angle evaporations in order to avoid coating the front transported mirror (the one facing the parabolic mirror). Note that the laser resonator as shown in Fig. 1 consists of two transported mirrors and no cleaved mirror is used. After fabrication, the rear transported mirror is coated by PSG/Au layers, while the front one is only covered by the PSG of an estimated 0.17-μm thickness.
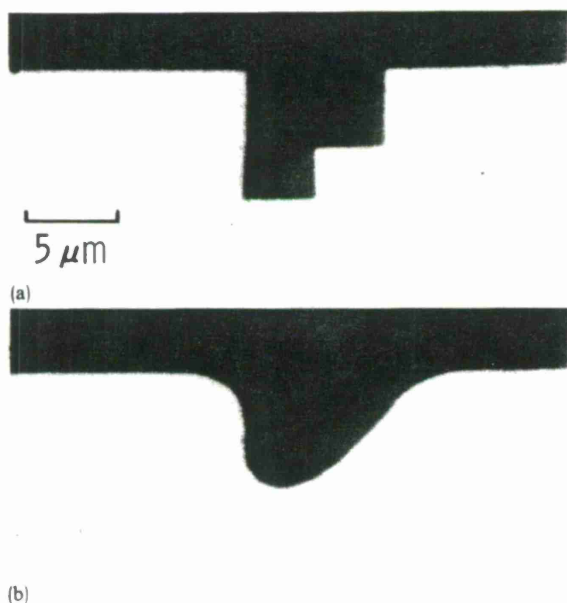

(b)

FIG. 3. Optical micrographs of the etched structures from wafers 693: (a) before and (b) after the mass transport. The GaInAsP layers have been stained and appear as dark lines in these photographs. In this wafer, the mass transport has been carried out at 740 °C.
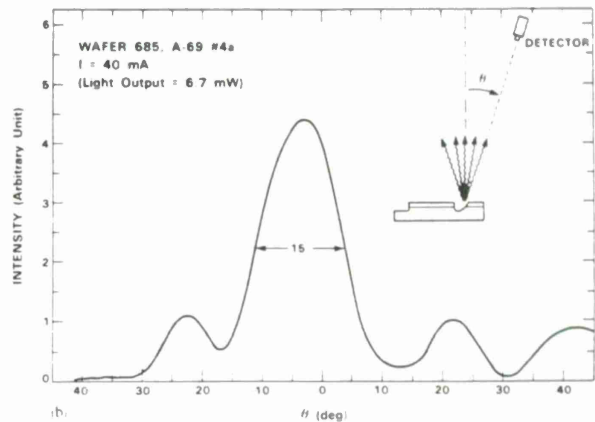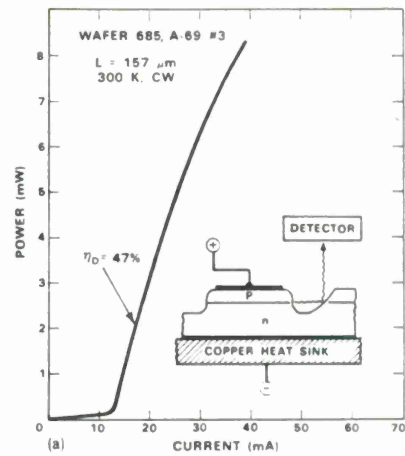

FIG. 4. Characteristics of the surface-emitting lasers: (a) light output vs current and (b) far-field pattern. The lasers are mounted p side up on copper heat sinks as indicated in the insert in part (a).

Surface-emitting lasers with low threshold current and high efficiency have been obtained with good yield. For example, 70% of the 26 devices tested without preselection from wafer 685 show pulsed threshold currents of 12–18 mA. The active region dimensions measured on this wafer are 0.20-μm thickness, 1.1–2.0-μm width, and 157-μm length (the distance between the transported mirrors). Four devices have been mounted p side up on copper heat sinks and all show room-temperature cw operation (with no increase in threshold current) and very similar surface-emitting far-field patterns. Figure 4(a) shows a cw light-output versus current characteristic in which an initial differential quantum efficiency of 47% is seen.

A far-field pattern is shown in Fig. 4(b) in which a main lobe of 15° angular width is seen. Other devices show the angular widths as small as 12°. These far-field patterns are considerably narrower than the corresponding ones of the conventional edge-emitting lasers (typically $\geqslant 30°$, see, for example, Refs. 9–13) and are close to the diffraction-limited angular width estimate from the present parabolic mirror size. (In wafer 685 the parabolic mirrors are made from a stair structure with t_1 of 2.7 μm, t_2 of 2.2 μm, and s of 2.5 μm.) The present far-field patterns typically show $\approx 5°$ deviations from the exact vertical direction and could be improved by a more precise control of the stair structure. Some of the side lobes seen in Fig. 4(b), especially the one at large angle, are possibly due to light scattered off the rounded

Z. L. Liau and J. N. Walpole   116

32

edges of the parabolic mirror and light that escapes the parabolic mirror due to the large beam divergence of the buried-heterostructure laser output. One solution to these problems is to use a larger parabolic mirror. The latter is desired also for achieving a still narrower diffraction-limited beam. However, further experiments with thicker cap layers and higher mass-transport temperatures are needed for the successful fabrication of larger parabolic mirrors.

An essentially single-longitudinal-mode operation within an approximately 10-mA current range has been observed. At 30 mA the device of Fig. 4(b) shows at $\lambda = 1.3393$ μm a dominant mode greater than 125 times the side modes which are 15 Å spaced. This degree of mode purity was never observed in our previously reported buried-heterostructure lasers[5,8] and can possibly be attributed to the fact that the present devices have a relatively short cavity, a heavier p doping, one mirror reflectively coated and the other (moderately) antireflectively coated.[14,15]

It should be noted that the present surface-emitting lasers have all mirrors fabricated by the mass-transport technique and show encouragingly low threshold and high efficiency comparable to the best of the conventional cleaved-mirror edge-emitting lasers (see, for example, Refs. 8, 12, and 13). Moreover, these device characteristics are obtained even though the wafers have been subjected to considerably higher temperatures than used before for mass transport. A potential problem is Zn diffusion away from the heavily doped cap layer. Although a recent depth-profiling study[16] on a sample heated to 690 °C showed no appreciable Zn diffusion, more experiments are needed to fully investigate the situation at the still higher temperatures used in this work. Finally, as mentioned above, mirrors capable of deflecting the laser beam to other prescribed directions can be fabricated by using the present technique but with different designs of the stair structure.

In conclusion, a surface-emitting GaInAsP/InP laser has been developed and is the first such laser with performance as good as the conventional edge-emitting ones. The availability of good surface-emitting diode lasers is very promising for a wide variety of new applications in integrated optoelectronics. In addition, the present laser is the first one in which all mirrors are fabricated by chemical etching and mass transport and is attractive for large-scale production purposes.

[1]K. Iga, H. Soda, T. Terakado, and S. Shimizu, Electron. Lett. **19**, 457 (1983); and earlier works cited therein.

[2]K. Iga, S. Ishikawa, S. Ohkouchi, and T. Nishimura, Appl. Phys. Lett. **45**, 348 (1984).

[3]See. For example, H. C. Casey and M. B. Panish, *Heterostructure Lasers* (Academic, NY, 1978), Part A, pp. 100–103.

[4]Y. Itaya, T. Matsuoka, Y. Nakano, Y. Suzuki, K. Kuroiwa, and T. Ikegami, Electron. Lett. **18**, 1006 (1982).

[5]Z. L. Liau, J. N. Walpole, and D. Z. Tsang, Appl. Phys. Lett. **44**, 945 (1984); Paper TuC5, Technical Digest, Seventh Topical Meeting on Integrated and Guided-Wave Optics, Optical Society of America, 1984. A recent recalibration of our Ge detector shows that the output power and differential quantum efficiency values reported in this reference should be multiplied by 1.20–1.26.

[6]L. A. Coldren, K. Furuya, and B. I. Miller, J. Electrochem. Soc. **130**, 1918 (1983).

[7]Z. L. Liau and J. N. Walpole, Appl. Phys. Lett. **40**, 568 (1982).

[8]Z. L. Liau, J. N. Walpole, and D. Z. Tsang, IEEE J. Quantum Electron. **QE-20**, 855 (1984).

[9]Y. Itaya, Y. Suematsu, S. Katayama, K. Kishino, and S. Arai, Jpn. J. Appl. Phys. **18**, 1795 (1979).

[10]M. Hirao, A. Doi, S. Tsuji, M. Nakamura, and K. Aiki, J. Appl. Phys. **51**, 4539 (1980).

[11]R. J. Nelson, P. D. Wright, P. A. Barnes, R. L. Brown, T. Cella, and R. G. Sobers, Appl. Phys. Lett. **36**, 358 (1980).

[12]H. Ishikawa, H. Imai, T. Tanahashi, K. Hori, and K. Takahei, IEEE J. Quantum Electron. **QE-18**, 1704 (1982).

[13]I. Mito, M. Kitamura, K. Kobayashi, S. Murata, M. Seki, Y. Odagiri, H. Nishimoto, M. Yamaguchi, and K. Kobayashi, IEEE J. Lightwave Technol. **LT-1**, 195 (1983).

[14]T. P. Lee, C. A. Burrus, J. A. Copeland, A. G. Dentai, and D. Marcuse, IEEE J. Quantum Electron. **QE-18**, 1101 (1982).

[15]J. N. Walpole and L. J. Missaggia (unpublished). In this reference, evidence has been obtained that the mirror coatings improve the mode purity and has been interpreted as due to an increase of the traveling-wave component in the laser cavity. (For the detrimental effect of the standing wave on the mode purity, see the theory of Lee *et al.* in Ref. 14.).

[16]P. Besomi, J. Degani, and R. B. Wilson, J. Appl. Phys. **55**, 1135 (1984).

33

APPENDIX C

35

A novel GaInAsP/InP distributed feedback laser

Z. L. Liau, D. C. Flanders,[a] J. N. Walpole, and N. L. DeMeo

Lincoln Laboratory, Massachusetts Institute of Technology, Lexington, Massachusetts 02173-0073

GaInAsP/InP distributed feedback lasers have been fabricated with a simple new design in which the grating is etched into the top of a mass-transported buried heterostructure. Single-frequency operation with sidemodes lower than − 32 dB and threshold currents as low as 16 mA have been achieved.

Recently, considerable effort has been devoted to the development of GaInAsP/InP distributed feedback (DFB) lasers for use as stable single-frequency sources in fiber optic communications and has resulted in devices with good performance.[1–9] However, fabrication of these devices has been rather involved, requiring up to three epitaxial growth runs and a waveguide with four or more layers in which the thickness of each layer has to be correctly adjusted. In this work, we describe a novel device design which offers high performance and considerable fabrication simplicity.

As illustrated in Fig. 1, the present device consists of a mass-transported buried heterostructure[10,11] with a thin *p*-InP cap layer and a wide mesa on which a grating corrugation is etched in the middle with Au/Zn alloyed contacts formed on each side. Sufficient coupling between the guided mode and the grating corrugation occurs if the InP cap layer is approximately 1 μm in thickness. The Au/Zn alloyed contacts are formed on the sides in order to avoid interactions with the guided mode.

The device fabrication starts with a liquid phase epitaxially grown GaInAsP/InP double heterostructure wafer (with an active layer of 0.16 μm in thickness) similar to those used previously[10,11] except that the InP cap layer (doped to $p \simeq 5 \times 10^{17}$ cm^{-3}) is only 1.0 ± 0.2 μm in thickness. The buried heterostructure (with an active region width no greater than approximately 2 μm) is formed using a previously described chemical etching and mass-transport procedure.[10,11] Then, the first-order grating corrugation with a periodicity of 2028 Å and tooth height of approximately 2500 Å is formed by using contact x-ray lithography[12] (with a holographically generated mask pattern) and ion-beam-assisted etching using chlorine gas.[13] The wafer is subsequently coated with a phosphosilicate glass (PSG) layer of 0.4-μm thickness (not shown in Fig. 1) and a pair of stripe openings is defined in the PSG on top of the laser mesa by photolithography and chemical etching. Au/Zn alloyed contacts are then formed in these openings. (No openings are made in regions designed for the unpumped sections.) The rest of the metallization and dicing procedures are similar to those described previously.[10] Each finished device has a cleaved front facet where the output power is measured. The rear end is either cleaved or saw cut. The devices are first tested for their pulsed threshold currents and then mounted *p* side up on copper heatsinks for cw operation and spectral examination.

Devices fabricated with a relatively long cavity (546 and 241 μm for pumped and unpumped sections, respectively)

and saw-cut rear end show room-temperature pulsed threshold currents as low as 16 mA. Figure 2 shows cw emission spectra of a device just above its lasing threshold. As evident in Fig. 2(a), the dominant lasing mode with a wavelength of 1.3098 μm is located on the shorter-wavelength side of the apparent spontaneous emission spectrum and is a strong indication that the device is lasing in a DFB mode, since the Fabry–Perot modes should be located on the other side of the spontaneous spectrum where the gain maximum occurs. This is confirmed by the Fabry–Perot mode operation at wavelengths of 1.33–1.34 μm observed in shorter devices cleaved from the same wafer but without the unpumped section and saw-cut end, as indicated in Fig. 2(a). (Since the present DFB resonance wavelength is approximately 260 Å away from the gain maximum, the Fabry–Perot mode can have a lower threshold current in devices without the unpumped section and saw-cut end.) Figure 2(b) shows a similar spectrum at 10.6 °C and on different scales. Note the threshold current drops to 31 mA. The series of peaks are likely the DFB modes with the dominant one just outside the stop band.[1,2]

At higher currents, the dominant mode continues to grow, and the other DFB modes are at − 37 dB when the current is 60 mA (which is approximately 1.54 times the threshold current I_{th}) as shown in Fig. 3. However, a pair of modes of unknown origin with a − 32 dB intensity is observed at ± 50 Å of the dominant DFB mode as evident in Fig. 3.

Shorter devices with smaller unpumped sections and both ends cleaved show room-temperature cw threshold currents as low as 13.5 mA but with more complicated mode behaviors. A device with pumped and unpumped sections of 318 and 152 μm, respectively, showed a cw threshold current of 16 mA at room temperature and single-frequency
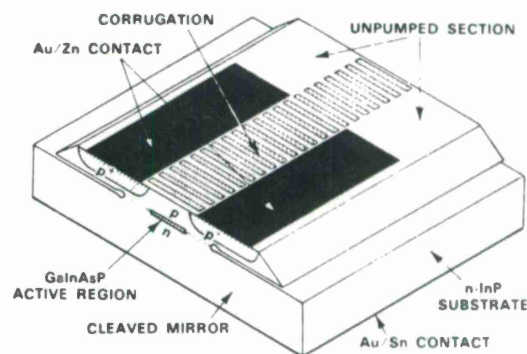

FIG. 1. Schematic drawing of the present GaInAsP/InP distributed feedback laser.

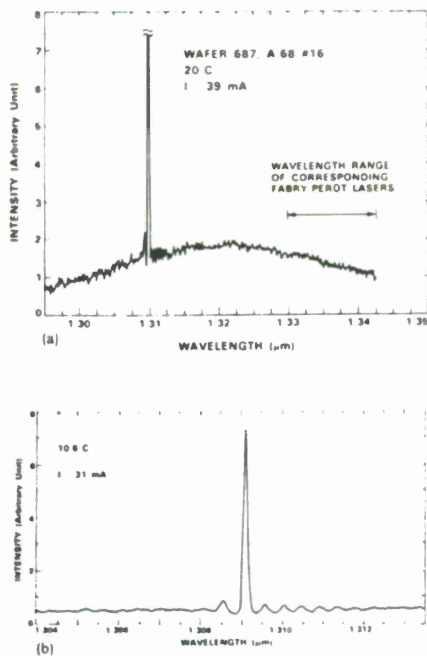[a] Present address: Lasertron, Inc., Burlington, Massachusetts.

37

FIG. 2. Emission spectra of one device just above the lasing threshold at (a) 20 °C and (b) 10.6 °C. Part (a) shows that the lasing modes are located on the shorter-wavelength side of the apparent spontaneous emission spectrum. The expanded wavelength scale in part (b) shows more details of the lasing spectrum.

operation (with sidemodes estimated at -30 dB) up to at least $2.5I_{th}$ (with an output power of 2.8 mW) but with a mode hop from $\lambda = 1.3054$ to 1.3092 μm at $1.6I_{th}$. Other devices with little or no unpumped sections lase in Fabry–Perot modes in the spectral region of 1.33–1.34 μm but still show considerably better mode purity than similar devices fabricated without the grating. (The latter also lase at wavelengths of 1.33–1.34 μm.)

The long devices with unpumped sections and saw-cut rear ends clearly show that good DFB lasers can be obtained with the present new design, even though the DFB resonance wavelength is some 260 Å away from the gain maxi-
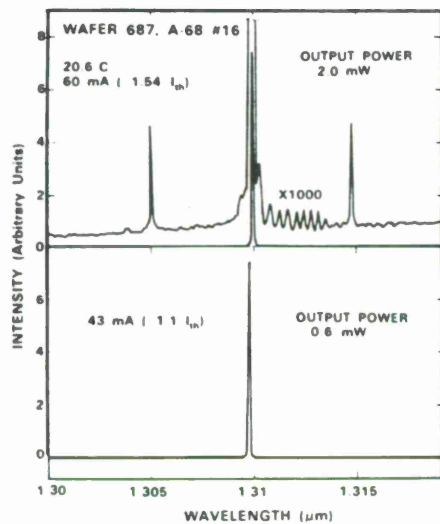

FIG. 3. Emission spectra of the device at 20.6 °C and two different currents above threshold. Note that at $I = 1.54I_{th}$ the sidemodes are lower than -32 dB.

mum. In fact, the 16-mA threshold current achieved in this work is already comparable to the lowest reported to date for the DFB diode lasers.[3] Still lower threshold currents can possibly be achieved when the DFB resonance wavelength and the gain maximum are better matched. Furthermore, it is worth noting that the present device is considerably simpler than more conventional ones[1–9] in terms of the waveguide and current-confinement structures and fabrication procedures. In particular, the grating is fabricated after the wafer growth is completed. This not only avoids the problems associated with growth over the grating[14–16] but also allows the wafer to be more thoroughly characterized before the grating is fabricated. To our knowledge, the present device is the first DFB laser of III-V compound semiconductors fabricated with grating placed on top of the cap layer, although a similar configuration has previously been used in a IV-VI laser.[17]

One potential problem of the present device is a possible leakage current I_H flowing through the InP pn homojunctions in the transported regions.[11] (The homojuctions are illustrated as dashed line segments in Fig. 1.) This current leakage has previously been analyzed for other mass-transported buried-heterostructure lasers and has been shown to be capable of causing a saturation of light output at high current.[11] A similar analysis has been carried out for the present structure,[18] in which the current I_Q flowing from the Au/Zn contacts to the quaternary active region and the corresponding voltage distribution are modeled by using a conformal mapping technique, as illustrated in Fig. 4. This analysis yields the forward-bias voltage along the homojunctions which can in turn be used to estimate I_H. For small values of I_Q the calculated I_H is negligible, but its importance grows with increasing I_Q. The value of I_Q when $I_H = 0.1I_Q$ is designated as I_1 and has been calculated for various device parameters, e.g., $I_1 = 74$ mA is obtained for the device of Fig. 4. I_1 can be increased considerably by using a higher p doping, narrower transported regions, a closer alignment of the Zn-diffused p^+ regions to the quaternary, or a larger pumped-section length. It is worth noting that, if the device were fabricated with an n-type mesa on a p-type substrate, there would be negligible voltage buildup due to high conductivity of n-type InP. However, the p doping on the substrate side would need optimization in order to enable very high current operation.

In conclusion, a GaInAsP/InP DFB laser has been realized in a simple new design in which the grating is fabricated on top of a mass-transported buried heterostructure.

FIG. 4. Calculated current and voltage distributions near the active region in the present structure. The dashed curves are the streamlines of the current flowing into the active region. The solid curves are the equipotentials with the numbers labeling the voltage values in volts. This analysis helps design the device for operation without significant current leakage through the InP pn homojunctions (by keeping the voltages sufficiently low).

38

Threshold currents as low as 16 mA have been obtained, and still lower threshold current can possibly be achieved when the DFB resonance wavelength and the gain maximum are better matched. Further optimization of the doping scheme, the transported region width, and ohmic contact alignment is needed for high-power capability.

[1]K. Utaka. S. Akiba, K. Sakai, and Y. Matsushima, IEEE J. Quantum Electron. QE-20, 236 (1984); and references therein.

[2]Y. Itaya, T. Matsuoka, K. Kuroiwa, and T. Ikegami, IEEE J. Quantum Electron QE-20, 230 (1984); and references therein.

[3]H. Okuda, Y. Hirayama, J. Kinoshita, H. Furuyama, and Y. Uematsu, Electron. Lett. 19, 941 (1983).

[4]L. D. Westbrook, A. W. Nelson, P. J. Fiddyment, and J. S. Evans, Electron. Lett. 20, 225 (1984).

[5]M. Kitamura, M. Yamaguchi, S. Murata, I. Mito, and K. Kobayashi, Electron. Lett. 20, 595 (1984); and references therein.

[6]B. Broberg, F. Koyama, Y. Tohmori, and Y. Suematsu, Electron. Lett. 20, 692 (1984).

[7]S. Tsuji, A. Oishi, Y. Kashiwada, N. Chinone, Y. Fujisaki, M. Hirao, and T. Kajimura, Technical Digest, Ninth IEEE International Semiconductor Laser Conference, Rio de Janeiro, 1984, p. 12.

[8]T. Watanabe, S. Suzaki, H. Katsuda, K. Takahashi, T. Nomura, T. Shimmen, and H. Osanai, Technical Digest, Ninth IEEE International Semiconductor Laser Conference, Rio de Janeiro, 1984, p. 68.

[9]T. L. Koch, T. J. Bridges, E. G. Burkhardt, R. A. Logan, L. F. Johnson, L. A. Coldren, P. J. Corvini, and W. T. Tsang, Technical Digest, Ninth IEEE International Semiconductor Laser Conference, Rio de Janeiro, 1984, post-deadline paper.

[10]Z. L. Liau and J. N. Walpole, Appl. Phys. Lett. 40, 568 (1982).

[11]Z. L. Liau, J. N. Walpole, and D. Z. Tsang, IEEE J. Quantum Electron. QE-20, 855 (1984).

[12]D. C. Flanders, J. Vac. Sci. Technol. 16, 1615 (1979).

[13]N. L. DeMeo, J. P. Donnelly, F. J. O'Donnell, M. W. Geis, and K. J. O'Connor, paper presented at the conference on Ion-Beam Modification of Materials '84, Ithaca, NY, 1984; Nucl. Instrum. Methods (to be published).

[14]A. W. Nelson, L. D. Westbrook, and J. S. Evans, Electron. Lett. 19, 34 (1983).

[15]J. Kinoshita, H. Okuda, and Y. Uematsu, Electron. Lett. 19, 215 (1983).

[16]H. Nagai, Y. Noguchi, T. Matsuoka, and Y. Suzuki, Jpn. J. Appl. Phys. 22, L291 (1983).

[17]J. N. Walpole, A. R. Calawa, S. R. Chinn, S. H. Groves, and T. C. Harman, Appl. Phys. Lett. 29, 307 (1976).

[18]The present calculation is somewhat different from that in Ref. 11 because of the device geometry and the relative importance of the electron drift current.

APPENDIX D

Single-Mode Optical Waveguides and Phase Modulators in the InP Material System

J. P. DONNELLY, N. L. DeMEO, F. J. LEONBERGER, S. H. GROVES,
P. VOHL, AND F. J. O'DONNELL

Abstract—The characteristics of several different single-mode optical waveguides in the InP material system are discussed. Slab-coupled rib waveguides in GaInAsP ($\lambda_{gap} \approx 1$ μm) epitaxial layers grown on InP have shown propagation losses as low as 1.7 cm^{-1} at 1.3 μm and 2.7 cm^{-1} at 1.15 μm. Oxide-confined InP rib guides fabricated using a lateral overgrowth technique have losses of about 1.5 cm^{-1} at 1.15 μm. Three-guide couplers have been made by fabricating three parallel oxide-confined guides in close proximity. InP p$^+$-n-n$^+$ guides capable of modulating TE-polarized radiation have been fabricated using epitaxial techniques and Be-ion implantation. By measuring the phase difference between the TE-like and TM-like modes as a function of applied voltage, an estimate of the r_{41} electrooptic coefficient in InP at 1.3 μm that is in good agreement with a previously reported value was obtained. Guides of this type should find use as the active components in InP switches and interferometers.

Fig. 1. Transmission versus length for single-mode GaInAsP rib waveguides.

BOTH low-loss, single-mode optical waveguides and waveguides in which the effective index can be modulated via the electrooptic effect are necessary components of semiconductor integrated-optic couplers, switches, and modulators [1]–[13]. There is much current interest in developing such devices in the InP material system because of their compatibility with 1.3–1.5 μm sources. In this paper, the characteristics of several different single-mode rib waveguides fabricated in the InP material system are presented. These include GaInAsP slab-coupled rib waveguides, oxide-confined InP rib guides, and p$^+$-n-n$^+$ InP rib guides capable of phase modulating TE polarized radiation.

Single-mode GaInAsP rib waveguides, as shown schematically in the insert in Fig. 1, were fabricated in n-type Ga$_{0.04}$In$_{0.96}$As$_{0.10}$P$_{0.90}$ layers ($\lambda_{gap} \approx 1$ μm) grown by liquid phase epitaxy (LPE) on Fe-doped InP substrates of (100) orientation. A special pregrowth baking procedure was used to reduce the background carrier concentration and thus minimize optical loss [14]. The net carrier concentration in the grown layer was in the $(2-5) \times 10^{15}$ cm^{-3} range, with mobilities at room temperature and 77 K of ~4500 and 25 000 cm^2/V · s, respectively. The waveguides, which were formed by standard photolithographic and wet-chemical techniques, were oriented for propaga-
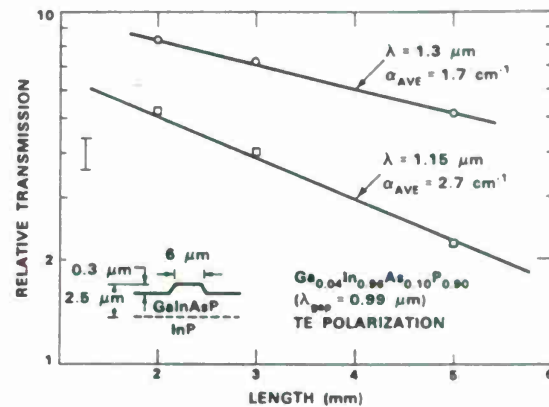
tion in an (01$\bar{1}$) direction. The quaternary layer thickness was typically 2.5 $\pm$ 0.2 μm. The guide width and etch depth were chosen to give single-mode operation [15]. Typical guide dimensions are shown in Fig. 1. To determine the propagation loss, transmission through several different lengths of the same sample was measured for a number of guides using an end-fired coupling technique. As shown in Fig. 1, single-mode losses as low as 1.7 cm^{-1} at 1.3 μm and 2.7 cm^{-1} at 1.15 μm have been measured for both TE and TM polarization. Band tailing in the quaternary layer and/or rib-edge roughness could be responsible for the higher loss at 1.15 μm. The losses at 1.3 μm are comparable to those obtained by Bornholdt *et al.* [16] but somewhat higher than the 4 dB/cm (≈ 1 cm^{-1}) obtained by Fujiwara *et al.* [17] using a double-heterojunction waveguide. The latter result may indicate that rib-edge roughness is responsible for a significant portion of the loss in the rib-guides reported in this paper.

Single-mode rib waveguides of a second type, as shown schematically in Fig. 2, were fabricated in epitaxial InP layers grown over oxide-coated InP substrates. To form these oxide-defined InP guides, a (100) n$^+$-InP substrate was coated with 0.3 μm of phosphosilicate glass (PSG), stripe openings were etched in the PSG, and an InP layer was grown by vapor phase epitaxy, using the InP-PCl$_3$-H$_2$ process. For the reasons discussed below, the stripe openings were oriented at an angle of 30° to the [01$\bar{1}$] direction in the plane of the substrate surface. Under the experimental conditions employed, a single-crystal layer with the same orientation as the substrate was obtained because nucleation occurred only where the substrate was exposed
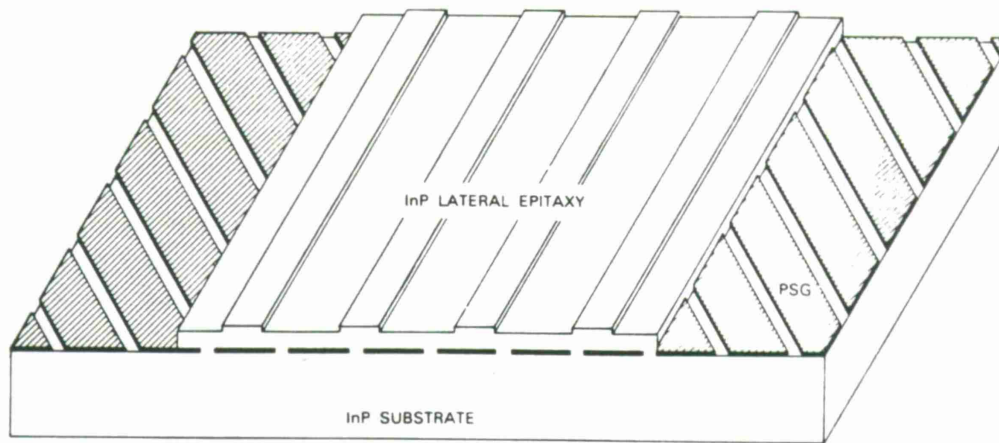
Fig. 2. Schematic drawing of InP oxide-confined guides formed on a wafer in which the angle of the phosphosilicate glass (PSG) stripe openings is optimized for continuous growth and the guides are oriented normal to a cleavage plane.

within the stripe openings. This was followed by lateral growth over the intervening oxide stripes until the growth originating within adjacent stripe openings merged to form a continuous layer, after which vertical growth took place in the usual manner until the layer reached the desired thickness [18]. The InP epitaxial layer was n-type with a carrier concentration in the low 10^{14} cm^{-3} range. Photolithographic and wet-chemical etching techniques were then used to fabricate ribs oriented normal to the $(01\bar{1})$ cleavage plane, and waveguides of the desired length were prepared by cleaving the epitaxial layer and the substrate. As shown in Fig. 2, each guide crossed a large number of the 30° stripe openings in the PSG.

The propagation loss of the oxide-defined InP waveguides was measured by determining the transmission of several different lengths of the same sample. The loss measured at 1.15 μm for TE polarization was 1.5 cm^{-1} for 9 μm wide guides etched 1 μm deep in a 5 μm thick InP layer grown over a PSG film with 3 μm wide stripe openings spaced at intervals of 50 μm. Although large, these guides appeared to be single-moded, which is in agreement with Marcatili's slab-coupled waveguide theory [15]. One of the lowest losses so far reported for single-mode semiconductor waveguides, 0.5 cm^{-1} at 1.06 μm, has been obtained for oxide-defined GaAs rib guides also fabricated in epitaxial layers prepared by lateral overgrowth on oxide-coated (100) substrates [19]. In contrast to the InP waveguides, the GaAs guides were parallel to the stripe openings in the oxide, which were formed at an angle of $\sim 10°$ to the [011] direction. For angles in the 10° range, the ratio of lateral to vertical growth rates is only about one-third as high for InP as for GaAs. The reduction in this ratio results in a corresponding reduction in the maximum width of oxide stripes over which continuous InP layers thin enough for fabricating single-mode waveguides can be grown. For practical integrated optics applications, however, the oxide stripes should be as wide as possible. In order to increase the maximum permitted stripe width, the angle chosen for InP overgrowth was 30°, which gives the highest ratio of lateral to vertical growth for (100) InP substrates. The rib guides were oriented normal to the

$(01\bar{1})$ plane to allow end-fired coupling into cleaved faces. Although each guide therefore crosses many stripe openings, the low overall loss measured for the guides shows that the loss per opening was extremely low.

Three-guide couplers were made by fabricating three parallel oxide-confined InP rib guides in close proximity [20] on a 4.5 μm thick epitaxial layer grown over oxide stripes as described above for the single guides. These devices had 5 μm wide guides separated by 5 μm and were etched to 0.8 μm deep. The coupling length, defined as the length necessary for power input to the center guide to be equally divided between the two outside guides, was determined by measuring the relative power in the three guides for several sample lengths. The coupling length at 1.3 μm for TE polarization was found to be ~ 6.4 mm. A photomicrograph of the output face of a device cleaved to this length is shown in Fig. 3 along with a photograph of the near-field output intensity pattern. Here 95 percent of the input power has been transferred equally to the outside guides.

In addition to being used for the formation of oxide-defined InP rib waveguides, the lateral growth of InP over oxide was also employed for the fabrication of inverted rib waveguides. Fig. 4 is a photomicrograph of the cleaved end of such a guide. To form these inverted guides, a (100) InP substrate was etched to form grooves oriented at an angle of 10° to the [011] direction in the plane of the surface. The substrate was coated with SiO$_2$, and a stripe opening also oriented at 10° was etched in the SiO$_2$ between each pair of grooves. The angle of 10° was selected to obtain the best compromise between maximizing the oxide stripe width and minimizing the angle between the waveguides and the cleaved face for end-fired coupling. An InP layer was then grown by vapor phase epitaxy, using the InP-PCl$_3$-H$_2$ process. Nucleation again occurred only where the substrate was exposed within the stripe openings, after which lateral growth took place over the oxide and down into the grooves. After the growths from the two sides of each groove merged to form a continuous layer over the SiO$_2$, vertical growth took place until the grooves were filled and a planar InP layer of the
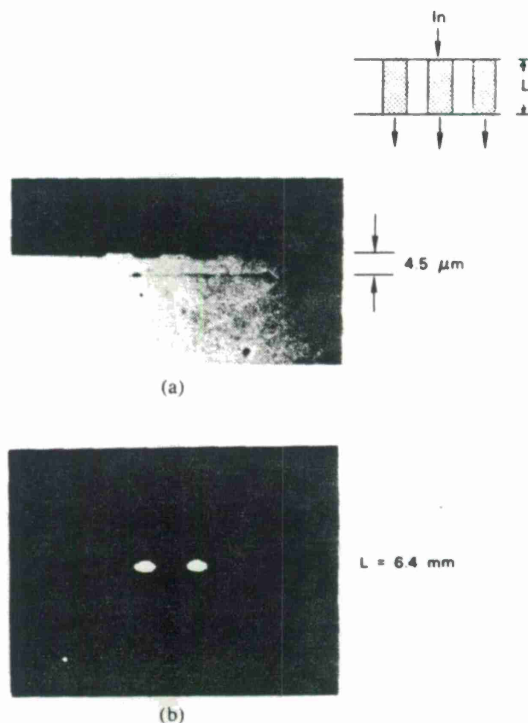
(a)

(b)

Fig. 3. (a) Photomicrograph of output face of InP oxide-confined three-guide coupler. The oxide film under the guiding layer is visible. (b) Photograph of near-field output intensity pattern obtained when light was incident on the center guide; 95 percent of the light has coupled to the outside guides.
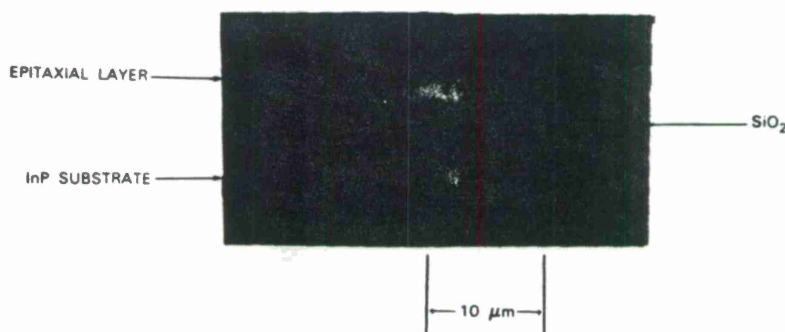

Fig. 4. Photomicrograph of oxide-confined single-mode InP optical waveguide with planar inverted rib structure.

desired thickness was formed. Finally, the end faces were formed by cleaving. Although guiding was obtained, it was not sufficiently single-moded to permit reliable loss measurements.

Waveguide modulators were formed by fabricating InP rib waveguides incorporating a p-n junction capable of being reverse-biased. A schematic cross section of a single-mode p^+-n-n^+ slab-coupled rib waveguide is shown in Fig. 5. The InP wafer used to fabricate these waveguides consisted of a (100) oriented n^+-substrate and a 5.5 μm thick n-type layer with a carrier concentration of $\approx 2 \times 10^{16}$ cm^{-3} grown by liquid phase epitaxy. To form the p^+ ribs, the wafer was implanted with a multienergy Be implant schedule and annealed at 750°C, which produced a 1.5 μm deep p^+ layer with a uniform carrier concentration of $\approx 2 \times 10^{18}$ cm^{-3} [21]. The junction depth obtained by implantation is uniform across a sample and reproducible from wafer to wafer. Rib waveguides approximately 5 μm wide were formed by etching through the p^+ implanted layer into the n epitaxial layer to a total depth of about 2 μm. The waveguides were oriented for propagation along an (01$\bar{1}$) direction. An SiO$_2$ layer was deposited on top of the wafer, and Au/Mg and Au/Sn ohmic contacts were applied to the p^+ ribs and the back of the n^+ substrate, respectively. The input and output faces of the waveguide were then cleaved. These p^+-n-n^+ InP waveguides are similar to GaAs waveguides recently used in a high-frequency interferometer [13], [22]. Although surface leakage currents are more of a problem in these p^+-n InP diodes than in similar GaAs diodes, their reverse leakage current is typically well below 1 μA at 25 V, as shown in Fig. 6. Above 25 V, breakdowns were soft and varied from
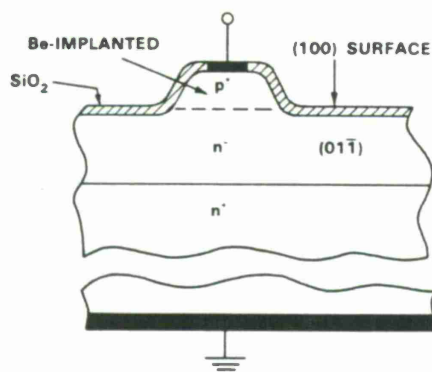
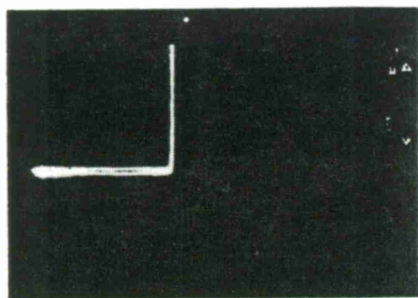Fig. 5. Schematic of single-mode p^+-n-n^+ InP slab-coupled rib waveguide.

Fig. 7. Relative output versus reverse bias of 5 mm long p^+-n-n^+ InP slab-coupled rib waveguide with equal amounts of TE-like and TM-like radiation excited at the input and an output analyzer parallel and perpendicular to the input polarization.

Fig. 6. Current–voltage characteristics of p^+-n-n^+ InP slab-coupled rib waveguide.

waveguide to waveguide, but at least 40 V reverse bias could be applied to all of the waveguides tested. These already good current–voltage characteristics should be improved by Si_3N_4 or polyimide passivation, which has greatly reduced leakage in InP photodiodes [23], [24].

To determine the modulation characteristics of a waveguide, radiation from a single-mode GaInAsP/InP double-heterojunction laser operating at 1.3 μm was passed through a polarizer and end-fired coupled into the cleaved end-face of the waveguide. The input radiation was polarized (nominally at 45° to the perpendicular) so that approximately equal amounts of TE-like and TM-like radiation were excited in the guide. The output of the waveguide was passed through an analyzer and focused on a Ge photodiode.

Fig. 7 shows the relative outputs of a 5 mm long waveguide versus reverse bias on the p^+-n junction with the analyzer either parallel or perpendicular to the input polarization. Both curves approximate an offset cosine function of applied voltage. The maximum output with the analyzer parallel to the input polarization (minimum output with the analyzer perpendicular to the input polarization) does not occur at zero bias, because at low fields the velocity of the TE-like mode is slower than that of the TM-like mode. Reverse biasing the p^+-n junction changes the refractive index in the plane of the junction, i.e., the (011) direction, but leaves the index perpendicular to the plane of the junction, i.e., the (100) direction, unaffected [25], [26]. The velocity of the TE-like mode, therefore, varies with reverse bias, while that of the TM-like mode is, at
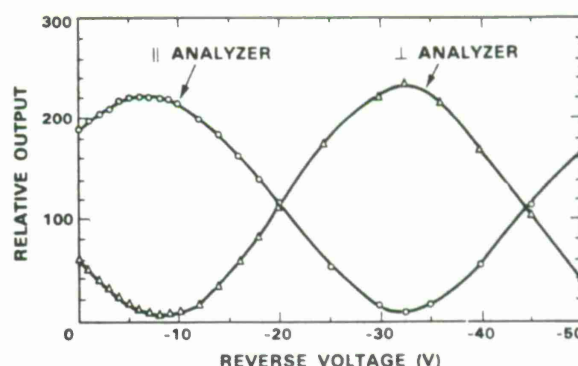
least to first order, not affected. This results in a change in phase of the TE-like mode relative to that of the TM-like mode at the output face, and produces the observed variation in relative output. The extinction ratio is about 16.5 dB. This relatively low value is most likely due to either slightly different amounts of TE- and TM-like radiation being initially excited in the guide or different mode losses, or both. Extinction ratios in couplers and interferometers, where only TE-like radiation is excited, should be considerably higher.

A voltage difference of about 25 V is required to produce a π-phase shift in the TE-like mode, i.e., to go from a maximum to a minimum in the relative output of either curve shown in Fig. 7. Using simple approximations for both the electric field shape in the p-n junction and the field shape of the TE-like optical mode, a rough estimate of $\approx 1.5 \times 10^{-10}$ cm/V for the electrooptic coefficient r_{41} was obtained from the measured voltage difference. This value is in remarkably good agreement with the stress-free and strain-free r_{41} values of 1.53×10^{-10} and 1.59×10^{-10} cm/V, respectively reported for InP at 1.306 μm by Suzuki and Tada [27]. In the present devices, however, in addition to the linear electrooptic effect, higher order effects, such as the quadradic electrooptic effect [28], may be playing a role in these devices, since the curves in Fig. 7 are not significantly more spread out at lower voltages than at higher voltages, where the overlap between the electric field and the optical field should be better.

The capacitance of these 5 mm long devices at a reverse bias of 20 V was about 2.5 pF. If the carrier concentration of the n epitaxial layer were reduced to less than 10^{15} cm^{-3}, the p^+-n-n^+ juonction would operate entirely in the punch-through mode. The capacitance would then be lower by at least a factor of 2 and vary less with applied voltage. In addition, the drive voltage required for a change in phase of π (180°) would decrease because of an increased overlap of the electric field with the optical mode. Although these waveguides were made relatively thick to permit easier excitation of equal amounts of the TE and TM modes, drive voltage requirements on switches or modulators could be reduced further by decreasing the epitaxial layer

thickness to ≤ 4 μm. A tradeoff between length and drive voltages is also possible. While the propagation loss of these guides was not measured in detail, a comparison of their transmission to that of guides of similar dimensions with known loss coefficients indicates the loss per unit length at 1.3 μm is on the order of 1.5–2.0 cm^{-1}.

In summary, several different types of InP and GaInAsP single-mode rib waveguides have been fabricated and evaluated. Slab-coupled rib waveguides fabricated in GaInAsP ($\lambda_{gap} \approx 1$ μm) layers grown on InP have shown losses of 1.7 cm^{-1} at 1.3 μm and 2.7 cm^{-1} at 1.15 μm. Oxide-confined InP waveguides and three-guide couplers have been fabricated by using a lateral overgrowth technique. These guides have losses of about 1.5 cm^{-1} at 1.15 μm. In addition, InP single-mode p^+-n-n^+ slab-coupled rib waveguides capable of phase modulating TE-polarized radiation have been fabricated by using Be-ion implantation. Waveguides of this type should prove useful in integrated optic two-guide coupler switches and interferometric modulators.

ACKNOWLEDGMENT

REFERENCES

[1] S. Somekh. E. Garmire, A. Yariv. H. L. Garvin, and R. G. Hunsperger. "Channel optical waveguide directional couplers," *Appl. Phys. Lett.*, vol. 22, pp. 46–47, Jan. 15, 1973.

[2] ——, "Channel optical waveguides and directional couplers in GaAs-imbedded and ridged." *Appl. Opt.*, vol. 13, pp. 327–330, Feb. 1974.

[3] J. C. Campbell. F. A. Blum, D. W. Shaw, and K. L. Lawley. "GaAs electrooptic directional-coupler switch," *Appl. Phys. Lett.*, vol. 27, pp. 202–204, Aug. 1975.

[4] F. J. Leonberger. J. P. Donnelly, and C. O. Bozler. "GaAs $p^+n^-n^+$ directional-coupler switch," *Appl. Phys. Lett.*, vol. 29, pp. 652–654, Nov. 15, 1976.

[5] ——, "Wavelength dependence of GaAs directional couplers and electrooptic switches." *Appl. Opt.*, vol. 17, pp. 2250–2254, July 15, 1978.

[6] J. C. Shelton. F. K. Reinhart, and R. A. Logan, "Rib waveguide switches with MOS electrooptic control for monolithic integrated optics in GaAs–Al$_x$Ga$_{1-x}$As." *Appl. Opt.*, vol. 17, pp. 2548–2555, Aug. 15, 1978.

[7] ——, "Characteristics of rib waveguides in AlGaAs," *J. Appl. Phys.*, vol. 50, pp. 6675–6687, Nov. 1979.

[8] A. Carenco, L. Menigaux, and P. L. Delpech. "Multiwavelength GaAs rib directional coupler switch with stepped 'DB' Schottky electrodes," *J. Appl. Phys.*, vol. 50, pp. 5139–5141, Aug. 1979.

[9] A. Carenco and L. Menigaux, "GaAs homojunction rib waveguide directional coupler switch," *J. Appl. Phys.*, vol. 51, pp. 1325–1327, Mar. 1980.

[10] A. Carenco, N. T. Linh, and L. Menigaux. "InP electro-optic directional coupler," *Appl. Phys. Lett.*, vol. 40, pp. 653–655, Aug. 15, 1982.

[11] O. Mikani and H. Nakogone, "Waveguide optical switch in InGaAsP/InP using free carrier plasma dispersion," *Electron. Lett.*, vol. 20, pp. 228–229, Mar. 15, 1984.

[12] P. Bauchmann, H. Kaufmann, H. Melchior, and G. Guekos, "Reactive ion etched GaAs optical waveguide modulators with low loss and high speed," *Electron. Lett.*, vol. 20, pp. 295–297, Mar. 29, 1984.

[13] J. P. Donnelly, N. L. DeMeo, G. A. Ferrante, K. B. Nichols, and F. J. O'Donnell, "An optical guided-wave gallium arsenide monolithic interferometer," *Appl. Phys. Lett.*, vol. 45, pp. 360–362, Aug. 15, 1984.

[14] S. H. Groves and M. C. Plonko, "Liquid-phase epitaxial growth of InP and InGaAsP alloys," *J. Cryst. Growth*, vol. 54, pp. 81–87, July 1981.

[15] E. A. J. Marcatili, "Slab-coupled waveguides," *Bell Syst. Tech. J.*, vol. 53, pp. 645–674, Apr. 1974.

[16] C. Bornholdt, W. Döldissen, D. Franke, N. Grote, J. Krausen, U. Niggerbrügge, N. P. Nolting. M. Schlak, and I. Tredke, "Passive optical GaInAsP/InP waveguides," *Electron Lett.*, vol. 19, pp. 81–82, Feb. 3, 1983.

[17] M. Fujiwara, A. Ajisawa. Y. Sugimoto, and Y. Ohta. "Gigahertz-bandwidth InGaAsP/InP optical modulator/switches with double-hetero waveguides," *Electron. Lett.*, vol. 20, pp. 790–792, Sept. 13, 1984.

[18] P. Vohl, C. O. Bozler, R. W. McClelland, A. Chu, and A. J. Strauss, "Lateral growth of single crystal InP dielectric films by orientation-dependent VPE," *J. Cryst. Growth*, vol. 56, pp. 410–422, Jan. 1982.

[19] F. J. Leonberger, C. O. Bozler, R. W. McClelland, and I. Melngailis. "Low-loss GaAs optical waveguides formed by lateral epitaxial growth over oxide," *Appl. Phys. Lett.*, vol. 38, pp. 313–315, Mar. 1, 1981.

[20] J. P. Donnelly, N. L. DeMeo, and G. A. Ferrante, "Three-guide optical couplers in GaAs," *J. Lightwave Technol.*, vol. LT-1, pp. 417–424, June 1983.

[21] J. P. Donnelly and C. A. Armiento, "Beryllium-ion implantation in InP and In$_{1-x}$Ga$_x$As$_y$P$_{1-y}$," *Appl. Phys. Lett.*, vol. 34, pp. 96–99, Jan. 1, 1979.

[22] J. P. Donnelly, N. L. DeMeo, G. A. Ferrante, and K. B. Nichols, "A high-frequency GaAs optical guided-wave electrooptic interferometric modulator," *IEEE J. Quantum Electron.*, vol. QE-21, pp. 18–21, Jan. 1985.

[23] V. Diadiuk, C. A. Armiento, S. H. Groves, and C. E. Hurwitz, "Surface passivation techniques for InP and InGaAsP," *IEEE Electron Device Lett.*, vol. EDL-1, pp. 177–179, Sept. 1980.

[24] N. Susa, H. Kanbe, H. Ando, and Y. Ohmachi, "Plasma enhanced CVD Si$_3$N$_4$ film applied to InP avalanche photodiodes," *Japan J. Appl. Phys.*, vol. 19, pp. L675–L678, Nov. 1980.

[25] S. Namba, "Electro-optical effect of zincblend," *J. Opt. Soc. Amer.*, vol. 51, pp. 76–79, Jan. 1961.

[26] A. Yariv, *Quantum Electronics.* New York: Wiley. 1967, pp. 300–306.

[27] N. Suzuki and K. Tada, "Electrooptic properties and Raman scattering in InP," *Japan J. Appl. Phys.*, vol. 23, pp. 291–295, Mar. 1984.

[28] H. G. Boch, J. Krasuen, H. P. Nolting, R. G. Logan, and F. K. Reinhart, "Electro-optical light modulation in InGaAsP/InP double heterojunction diodes," *Appl. Phys. Lett.*, vol. 42, pp. 692–694, Apr. 15, 1983.

REPORT DOCUMENTATION PAGE

1a. REPORT SECURITY CLASSIFICATION	1b. RESTRICTIVE MARKINGS
Unclassified	

2a. SECURITY CLASSIFICATION AUTHORITY	3. DISTRIBUTION/AVAILABILITY OF REPORT
2b. DECLASSIFICATION/DOWNGRADING SCHEDULE	Approved for public release; distribution unlimited.

4. PERFORMING ORGANIZATION REPORT NUMBER(S)	5. MONITORING ORGANIZATION REPORT NUMBER(S)
	ESD-TR-87-054

6a. NAME OF PERFORMING ORGANIZATION	6b. OFFICE SYMBOL (If applicable)	7a. NAME OF MONITORING ORGANIZATION
Lincoln Laboratory, MIT		Electronic Systems Division

6c. ADDRESS (City, State, and Zip Code)	7b. ADDRESS (City, State, and Zip Code)
P.O. Box 73 Lexington, MA 02173-0073	Hanscom AFB, MA 01731

8a. NAME OF FUNDING/SPONSORING ORGANIZATION	8b. OFFICE SYMBOL (If applicable)	9. PROCUREMENT INSTRUMENT IDENTIFICATION NUMBER
Rome Air Development Center	RADC/ESMS	F19628-85-C-0002

8c. ADDRESS (City, State, and Zip Code)	10. SOURCE OF FUNDING NUMBERS			
	PROGRAM ELEMENT NO.	PROJECT NO.	TASK NO.	WORK UNIT ACCESSION NO.
Griffiss AFB New York, NY 13440	62702F, 61102F	85		

11. TITLE (Include Security Classification)

Electrooptical Devices

12. PERSONAL AUTHOR(S)
Tsang, Dean Z. and Williamson, Richard C.

13a. TYPE OF REPORT	13b. TIME COVERED	14. DATE OF REPORT (Year, Month, Day)	15. PAGE COUNT
Annual Report	FROM 10/1/84 TO 9/30/85	1985, September, 30	58

16. SUPPLEMENTARY NOTATION

None

17.	COSATI CODES		18. SUBJECT TERMS (Continue on reverse if necessary and identify by block number)
FIELD	GROUP	SUB-GROUP	electrooptical devices GaAs interferometer modulator
			DFG laser GaInAsP/InP lasers
			surface-emitting laser buried heterostructure

19. ABSTRACT (Continue on reverse if necessary and identify by block number)

This report covers work carried out with support of the Rome Air Development Center during the period 1 October 1984 through 30 September 1985.

The frequency response of an optical guided-wave GaAs interferometer has been measured. The bandwidth of the interferometer biased at a null point was 2.2 GHz, limited by parasitics. A small-signal bandwidth of ≈3 GHz can be inferred from this measurement for the case where the interferometer is biased to a linear operating point. This is the highest bandwidth yet reported for a guided-wave GaAs modulator.

A surface-emitting GaInAsP/InP laser has been developed in which a monolithically integrated parabolic mirror is used to up-deflect the output of a buried-heterostructure laser. A threshold current as low as 12 mA and a differential quantum efficiency as high as 46 percent have been obtained.

GaInAsP/InP distributed feedback lasers have been fabricated with a simple new design in which the grating is etched into the top of a mass-transported buried heterostructure. Single-frequency operation with side modes lower than −32 dB and threshold currents as low as 16 mA has been achieved.

Single-mode InP p^+-n^--n^+ slab-coupled rib waveguides capable of phase modulating, TE-polarized, 1.3-μm radiation have been fabricated. These guides should prove useful in the fabrication of two-guide coupler switches and interferometric modulators.

20. DISTRIBUTION/AVAILABILITY OF ABSTRACT	21. ABSTRACT SECURITY CLASSIFICATION
☐ UNCLASSIFIED/UNLIMITED ☒ SAME AS RPT. ☐ DTIC USERS	Unclassified

22a. NAME OF RESPONSIBLE INDIVIDUAL	22b. TELEPHONE (Include Area Code)	22c. OFFICE SYMBOL
Lt. Col. Hugh L. Southall, USAF	(617) 981-2330	ESD/TML

DD FORM 1473, 84 MAR   83 APR edition may be used until exhausted.
All other editions are obsolete.